

The Choice of μ -Vinyliminium Ligand Substituents is Key to Optimize the Antiproliferative Activity of Related Diiron Complexes

Beatrice Campanella,^a Simona Braccini,^b Giulio Bresciani,^b Michele De Franco,^c Valentina Gandin,^c Federica Chiellini,^{b,†} Alessandro Pratesi,^b Guido Pampaloni,^b Lorenzo Biancalana,^{b,*} Fabio Marchetti^{b,*}

^a Istituto di Chimica dei Composti Organometallici, Consiglio Nazionale delle Ricerche, Via G. Moruzzi 1, I-56124 Pisa, Italy.

^b University of Pisa, Department of Chemistry and Industrial Chemistry, Via G. Moruzzi 13, I-56124 Pisa, Italy.

^c University of Padova, Department of Pharmaceutical and Pharmacological Sciences, Via F. Marzolo 5, I-35131 Padova, Italy.

*Corresponding Authors

lorenzo.biancalana@unipi.it; fabio.marchetti@unipi.it

https://people.unipi.it/fabio_marchetti/

[†] Deceased in March 2021

Abstract

Diiron vinyliminium complexes constitute a large family of organometallics displaying a promising anticancer potential. The complexes $[\text{Fe}_2\text{Cp}_2(\text{CO})(\mu\text{-CO})\{\mu\text{-}\eta^1\text{:}\eta^3\text{-C}(\text{R}^3)\text{C}(\text{R}^4)\text{CN}(\text{R}^1)(\text{R}^2)\}\text{CF}_3\text{SO}_3$ (**2a-c**, **4a-d**) were synthesized, assessed for their behavior in aqueous solutions (D_2O solubility, $\text{Log } P_{ow}$, stability in $\text{D}_2\text{O}/\text{DMSO-d}_6$ mixture at $37\text{ }^\circ\text{C}$ over 48 hours) and investigated for their antiproliferative activity against A2780 and A2780cisR ovarian cancer cell lines and the nontumoral one Balb/3T3 clone A31. Cytotoxicity data collected for 50 vinyliminium complexes were correlated with the structural properties (*i.e.*, the different $\text{R}^1\text{-R}^4$ substituents) using the Partial Least Squares (PLS) methodology. A clear positive correlation emerged between the octanol-water partition coefficient and the relative antiproliferative activity on ovarian cancer cell lines, both of which appear as uncorrelated to the cancer cell selectivity. However, the different effects played by the $\text{R}^1\text{-R}^4$ substituents allow to trace guidelines for the development of novel, more effective compounds. Based on these results, three additional complexes (**4p-r**) were designed, synthesized and biologically investigated, revealing their ability to hamper thioredoxin reductase enzyme (TrxR) and to induce cancer cell production of reactive oxygen species (ROS).

Keywords: anticancer metal drugs, diiron complexes, cytotoxicity, chemometric analysis, Partial Least Squares regression, mass spectrometry.

Introduction

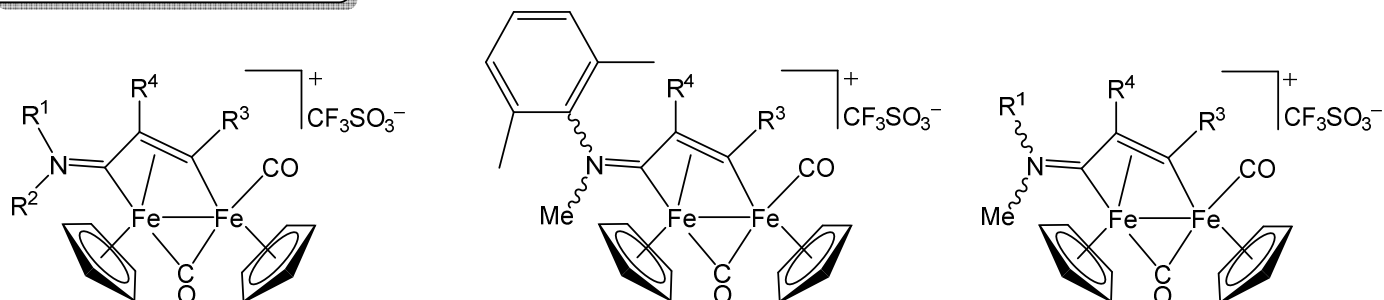
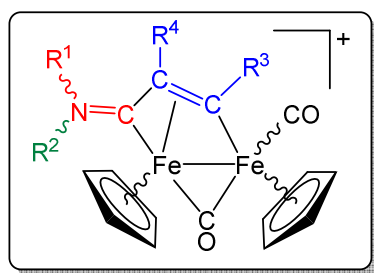
Transition metal compounds possess unique characteristics for potential medicinal applications,¹ and few square-planar platinum complexes have been widely used in clinical treatments against several types of tumors.² However, some limitations associated with the toxicity of platinum have put in motion the search for alternative drugs based on other metal elements and structures.³ An accurate

design of ligands and substituents is crucial to determine suitable physico-chemical pre-requisites, such as water solubility and stability, and eventually an optimal anticancer activity.^{4,5}

Iron complexes have attracted a huge interest for medicinal purposes,⁶ basically because iron is an endogenous element, and therefore its compounds are endowed with a relatively low toxicity;⁷ moreover, iron possesses two main adjacent oxidation states (i.e., +II and +III) and a relevant versatile redox activity which is key to the biological action. Ferrocene derivatives have been intensively investigated as anticancer agents, and they are generally believed to exert their antiproliferative activity by unbalancing the redox cell homeostasis through Fe^{II} to Fe^{III} oxidation.^{8,9} The {Fe₂Cp₂} core might be viewed as a dinuclear analogue of the ferrocene scaffold {FeCp₂}, and the easily available compound [Fe₂Cp₂(CO)₄] is an excellent starting material to access a plethora of diiron complexes with functionalized ligands occupying one bridging coordination site.¹⁰ This synthetic approach takes advantage from the cooperative effects provided by the two adjacent iron atoms, enabling unique reactivity patterns and the stabilization of uncommon organic fragments, otherwise not possible on related monometallic species.¹¹ In particular, the sequential displacement of two carbonyls from [Fe₂Cp₂(CO)₄] permits the assembly of isocyanide (CNR¹), alkyl cation ([R²]⁺) and alkyne (R³C≡CR⁴) units to afford a bridging vinyliminium ligand anchored to the two metal centers through uncommon {μ-η¹:η³} coordination mode (Scheme 1, inset).^{12,13} In correspondence to specific substituents R¹-R⁴, the resulting complexes may display two forms of stereoisomerism, *i.e.* *cis-trans* and *E-Z*, related to the mutual orientation of the Cp rings and the nitrogen substituents, respectively.^{12,14} The very general character and high regioselectivity of the alkyne insertion reaction, the commercial availability of normally easy-to-handle alkynes, the gram/multigram scale of the synthetic steps and the indefinite air-stability of the products in the solid state render diiron vinyliminium complexes (as triflate salts) a valuable and unusually numerous family of organometallics, of which over 100 members have been reported to date.

Recent studies revealed that this family of $[\text{Fe}^{\text{I}}\text{Fe}^{\text{I}}]$ complexes holds a promising anticancer potential: the compounds exhibit a tunable cytotoxic activity against cancer cells, and IC_{50} values in the nanomolar range have been recognized in A2780 and A2780cisR cell lines.^{15,16,17,18,19,20,21} Nevertheless, even the most cytotoxic compounds show a balanced hydrophilic/lipophilic character, regulated by the $\text{R}^1\text{-R}^4$ substituents.

The mechanism of action is presumably multimodal, however the interference of the drug with cell redox processes seems preponderant, being triggered inside the cell by both complex reduction and fragmentation routes, and involving the generation of ROS and the inhibition of TrxR, an important and ubiquitous flavoenzyme critically involved in the regulation of intracellular redox metabolism.²² The large structural variability of the vinyliminium ligand offers much opportunity in terms of structure-activity optimization. In this work, we report a simple chemometric approach to analyze the individual contributions of each substituent $\text{R}^1\text{-R}^4$ on the biological performance, pointing to the identification of the best combination(s). The list of analyzed complexes is shown in Scheme 1, including seven complexes for which biological data are presented here for the first time (i.e., **2a-c** and **4a-d**), along with some novelties in their preparation and spectroscopic characterization. Hence, the results of the chemometric analysis led us to design and synthesize complexes **4p-r** which were assessed for their cytotoxicity and ability to trigger ROS production and inhibit TrxR enzyme.



	R ¹ = R ²	R ³	R ⁴
2a*	Me	H	H
2b*	Me	SiMe ₃	H
2c*	Me	CO ₂ Me	H
2d ¹⁵	Me	Me	H
2e ¹⁵	Me	Ph	H
2f ¹⁸	Me	CH ₂ OMe	H
2g ¹⁵	Me	3-C ₆ H ₄ OH	H
2h ¹⁵	Me	4-C ₆ H ₄ CO ₂ H	H
2i ²⁰	Me	2-C ₆ H ₄ NH ₂	H
2j ²⁰	Me	3,5-C ₆ H ₃ (CF ₃) ₂	H
2k ²⁰	Me	4-C ₆ H ₄ Me	H
2l ²⁰	Me	4-C ₆ H ₄ F	H
2m ¹⁵	Me	1-Nap	H
2n ¹⁵	Me	3-thiophenyl	H
2o ¹⁵	Me	Me	Me
2p ¹⁵	Me	CO ₂ Me	CO ₂ Me
2q ¹⁵	Me	Ph	Ph
2r ¹⁶	Me	Me	SPh
2s ¹⁶	Me	Me	SeMe
3a ¹⁹	Bn	Me	H
3b ¹⁹	Bn	Me	Me

	R ³	R ⁴
4a*	H	H
4b*	SiMe ₃	H
4c*	CO ₂ Me	H
4d*	Et	H
4e ¹⁵	Me	H
4f ¹⁵	Ph	H
4g ¹⁵	CH ₂ OH	H
4h ¹⁸	CH ₂ OMe	H
4i ¹⁵	2-pyridyl	H
4j ²⁰	4-C ₆ H ₄ Me	H
4k ¹⁵	1-Nap	H
4l ¹⁵	3-thiophenyl	H
4m ¹⁵	Me	Me
4n ¹⁵	CO ₂ Me	CO ₂ Me
4o ¹⁵	Ph	SMe
4p*	ⁿ Pr	H
4q*	ⁿ Bu	H
4r*	(CH ₂) ₄ Me	H

	R ¹	R ³	R ⁴
5a ¹⁹	All	Me	H
5b ¹⁹	All	Ph	H
5c ¹⁹	All	Me	Me
6a ¹⁹	Anis	Me	H
6b ¹⁹	Anis	Ph	H
6c ¹⁹	Anis	Me	Me
7a ¹⁹	Cy	Me	H
7b ¹⁹	Cy	Ph	H
7c ¹⁹	Cy	Me	Me
8a ¹⁹	Bn	Me	H
8b ¹⁹	Bn	Ph	H
8c ¹⁹	Bn	Me	Me
8d ¹⁹	Bn	Et	Et
9a ¹⁹	2-Nap	Me	Me

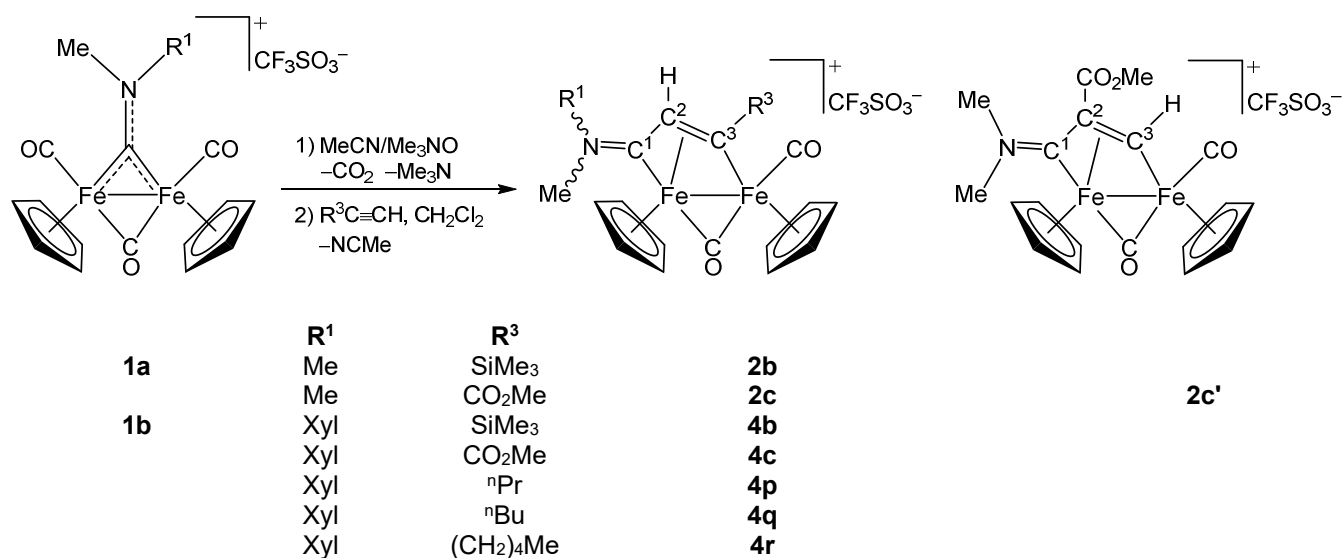
Scheme 1. Overview of complexes investigated for *in vitro* cytotoxic activity (Nap = naphthyl; Bn = CH₂Ph; All = CH₂CHCH₂; Anis = 4-C₆H₄OMe; Cy = C₆H₁₁). *Investigated in this work. Inset: general structure of diiron complexes with a bridging vinyliminium ligand obtained from stepwise isocyanide (red)/alkyl cation (green)/alkyne (blue) assembly.

Results and discussion

1. Synthesis, characterization and behavior in aqueous solutions.

Complexes **2a**, **4a**²³ and **4d**²⁴ were prepared following the published procedures. Instead, the synthesis of **2b-c** and **4b,c,p-r** was optimized with respect to the literature:^{13,14} it was performed at room

temperature and avoided the use of inert atmosphere (see Experimental for details). Thus, the parent diiron aminocarbonyl complexes underwent carbon monoxide/acetonitrile substitution by means of the trimethylamine N-oxide strategy;²⁵ then, alkyne η^2 -coordination^{13b,26} and successive insertion into the iron-carbonyl bond took place upon facile displacement of the labile nitrile ligand²⁷ (Scheme 2). Following chromatography on alumina, **2b-c** and **4b,c,p-r** were isolated as brown solids in 78-90 % yield. [Note: compounds **4p-r** were prepared and investigated after the biological studies and the statistical analyses comprising **2b-c** and **4b-d**, *vide infra*].



Scheme 2. Diiron μ -vinyliminium complexes investigated for *in vitro* cytotoxic activity in this work (Xyl = 2,6-C₆H₃Me₂).

Products prepared through the optimized synthetic procedure were characterized by CHNS analysis, IR and NMR spectroscopy (Figures S1-S11). Differently from what reported previously,¹⁴ **2c** was obtained in admixture with a minor amount of its isomer **2c'** (**2c/2c'** ratio = 3), the latter resulting from reverse insertion of the alkyne. The ¹H NMR resonance of the C³H proton is diagnostic for **2c'**, being considerably downfield shifted with respect to C²H in **2c** (δ = 12.81 ppm in **2c'**, 4.97 ppm in **2c**; acetone solution). This feature is consequence of the bridging alkylidene nature of C³ and is typically

observed in group 8 metal complexes containing a $\{\mu\text{-CH(R)}\}$ alkylidene moiety.^{13a,28} The peculiar formation of **2c'** is probably the consequence of the relatively low steric hindrance exerted by the iminium group combined with electronic effects of the $\{\text{CO}_2\text{Me}\}$ function. In all the other cases, reactions leading to the vinyliminium complexes were fully regiospecific, thus placing the alkyne substituent far away from the iminium, in agreement with the very general trend (see Introduction). A comparison of the NMR data of the complexes with the library of literature data on other $\text{Fe}_2\text{-}\mu\text{-vinyliminium}$ compounds evidences that **2b-c** and **4b-c** exist in solution exclusively in the *cis* form (with reference to the Cp ligands bound to Fe-Fe).¹⁵ As a matter of fact, the Cp resonances fall in the range 5.11 – 5.67 ppm, whereas *trans* isomers, when observed, display one Cp resonance at approximately 4.5 ppm.¹⁴ In addition, complex **4c** features *E-Z* isomerism, due to the different substituents on the iminium, with predominance of the *E* isomer. The *E* isomer is the only one recognized in the case of **4b**. Note that *E-Z* type isomers are easily distinguishable by looking at the resonances of one Cp ligand and the N-methyl, the latter falling at higher ^1H chemical shift in *E* with respect to *Z*.^{13a}

The trimethylsilyl unit in **2b** and **4b** was further characterized by ^{29}Si NMR spectroscopy: the related signal was found around 9.4 ppm, in comparison to -16.8 ppm observed in $\text{HC}\equiv\text{CSiMe}_3$; such strong downfield shift (*ca.* 26 ppm) may be ascribed to the bridging alkylidene nature of the adjacent C^3 (see above).²⁹

In view of the biological application, the water solubility of **2a-c** and **4a-d** was assessed at 21 °C in a saturated D_2O solution, by means of ^1H NMR spectroscopy. Moreover, octanol/water partition coefficients ($\text{Log } P_{\text{ow}}$) of the compounds were determined spectrophotometrically (see Experimental for details). Solubility data and partition coefficients are compiled in Table 1. Overall, the compounds show a fair to good solubility in water (0.7 - 14 mM range, except **4b**; cisplatin³⁰: 8.4 mM) and an amphiphilic character ($\text{log}_{10} P_{\text{ow}}$ between -0.9 and +0.5). The introduction of $\{\text{SiMe}_3\}$ led to an

expected,³¹ although not marked, decrease in water solubility and increase in lipophilicity (*e.g.* compare **2a/2b** and **4a/4b**). As previously noted,¹⁵ vinyliminium compounds featuring two methyl substituents on the nitrogen are more soluble in water and more hydrophilic than their methyl/xylyl counterparts.

Finally, the inertness of the diiron compounds in a D₂O/DMSO-*d*₆ 6:1 v/v mixture, following a 48 hour treatment at 37 °C in the presence of ambient light, was checked by ¹H NMR spectroscopy (Table 1). All compounds display a moderate inertness under the investigated conditions, given that *ca.* 80% of the starting material was present in solution at the end of the experiment. The brown precipitate formed over time is presumably iron oxide(s).^{15,32} It is worth noting that isomer ratios observed in the aqueous medium are in some cases considerably different from those ascertained in organic solvents; moreover some *E* to *Z* isomerization occurs during the 48 h, most notably in the case of **4c** and **4p**. The stability of **4q** was also assessed on a D₂O/DMSO-*d*₆ 6:1 v/v solution protected from the light, highlighting a negligible effect of light.

Table 1. Solubility in water (D₂O), octanol/water partition coefficient (Log *P*_{ow}) and % residual complex in aqueous solution after 48 hours at 37 °C for diiron compounds.

Complex	Solubility (D ₂ O, 21°C) [a]		Log <i>P</i> _{ow} [b]	% Residual complex (48 h, 37 °C, D ₂ O/DMSO- <i>d</i> ₆ 6:1 v/v) [a]
	mol·L ⁻¹	g·L ⁻¹		
2a	1.4x10 ⁻²	7.3	-0.77 ± 0.04	89
2b	4.4x10 ⁻³	2.6	-0.30 ± 0.03	85
2c + 2c' [c]	6.3x10 ⁻³	3.7	-0.88 ± 0.07	84
4a [c]	7x10 ⁻⁴	0.4	0.01 ± 0.04	81
4b [c]	< 3x10 ⁻⁴ [d]	< 0.2	0.5 ± 0.1	84 [e]
4c [c]	1.4x10 ⁻³	0.9	-0.1 ± 0.1	78
4d [c]	1.1x10 ⁻³	0.7	-0.08 ± 0.09	89
4p [c]	< 3x10 ⁻⁴ [d]	< 0.2	0.2 ± 0.1	74 [e]
4q [c]	< 3x10 ⁻⁴ [d]	< 0.2	0.66 ± 0.03	82 (84 ^[f]) [e]
4r [c]	< 3x10 ⁻⁴ [d]	< 0.2	0.87 ± 0.02	85 [e]

[a] Based on ¹H NMR spectroscopy, dimethylsulphone (Me₂SO₂) as internal standard, samples stored in the presence of ambient light. [b] Based on UV-Vis spectroscopy. [c] Data is referred collectively to all isomers. [d] Below the lowest value of quantitation. [e] D₂O/DMSO-*d*₆ 5:2 v/v solution. [f] In the absence of light.

2. Cytotoxicity studies and interaction with biomolecules.

The antiproliferative activity of **2a-c** and **4a-d** was assessed on the human ovarian carcinoma A2780 (cisplatin nonresistant) and A2780cisR (cisplatin resistant) cell lines and the noncancerous murine Balb/3T3 clone A31 cell line (Table 2). Cisplatin was used as a reference. In general, the investigated diiron complexes exhibit a cytotoxicity approximately correlating with the lipophilicity. In particular, the xylyl compounds **4b** and **4d** exhibit IC_{50} values, referred to the A2780 cell line, in low micromolar – nanomolar range. Compounds are substantially less active in the cisplatin resistant cell line, nevertheless the activity drop on going from A2780 to A2780cisR seems influenced by the iminium substituents, being in general less pronounced in the presence of the xylyl group and especially when $R^3 = H$. Data highlight a significant selectivity of the diiron complexes towards the cancer cell lines with respect to the selected nontumoral cell line. Overall, complex **4b** stands out among the series upon a comparison with cisplatin, with almost identical IC_{50} value on the A2780 cells and approximately ten-fold higher activity in the A2780cisR cells and ten-fold lower activity in the Balb/3T3 cells.

Table 2. IC_{50} values (μM) determined for iron compounds and cisplatin on human ovarian carcinoma (A2780), human ovarian carcinoma cisplatin-resistant (A2780cisR) and murine embryonic fibroblast (Balb/3T3 clone A31) cell lines after 72 hours exposure. Values are given as the mean \pm SD.

Complex	A2780	A2780cisR	Balb/3T3
2a	80 \pm 9	>100	>100
2b	4.6 \pm 0.6	41 \pm 3	>100
2c	17 \pm 3	78.9 \pm 1.4	>100
4a	3.6 \pm 0.5	9.2 \pm 0.5	41 \pm 4
4b	0.35 \pm 0.02	3.0 \pm 0.4	8.6 \pm 0.4
4c	14 \pm 3	39 \pm 3	55 \pm 11
4d	1.80 \pm 0.15	9 \pm 2	22 \pm 3
cisplatin	0.40 \pm 0.07	26 \pm 3	0.8 \pm 0.1

The most potent complex, **4b**, was selected for studying its reactivity with biomolecules. First, we examined through high-resolution mass spectrometry the interaction of **4b** with a dodecapeptide model (TrxR-pept) of thioredoxin reductase (TrxR). This model system is substantially cost-effective and was previously employed with success,³³ including on related diiron vinyliminium complexes.¹⁹ Following 24 hours of incubation at 37 °C, the spectrum showed a signal at m/z 1237.3195, ascribable to $[\text{TrxR-pept} + \text{Fe} - \text{H}]^+$, beyond the signals of unreacted TrxR-pept and its adducts with sodium and potassium (Figure 1). This outcome suggests that TrxR enzyme inhibition, via iron transfer made possible by intracellular disassembly of the diiron skeleton, may be involved in the mechanism of action of diiron bis-cyclopentadienyl carbonyl complexes.^{19,34}

On the other hand, an ESI-MS study revealed the inertness of **4b** towards Cytochrome c, employed as a model protein (see Figure S12). The absence of covalent bond formation with proteins was previously recognized on other diiron vinyliminium complexes,¹⁹ and seems related to the saturated coordination sphere around the metal centers, not allowing the binding of aminoacidic residues.³⁵

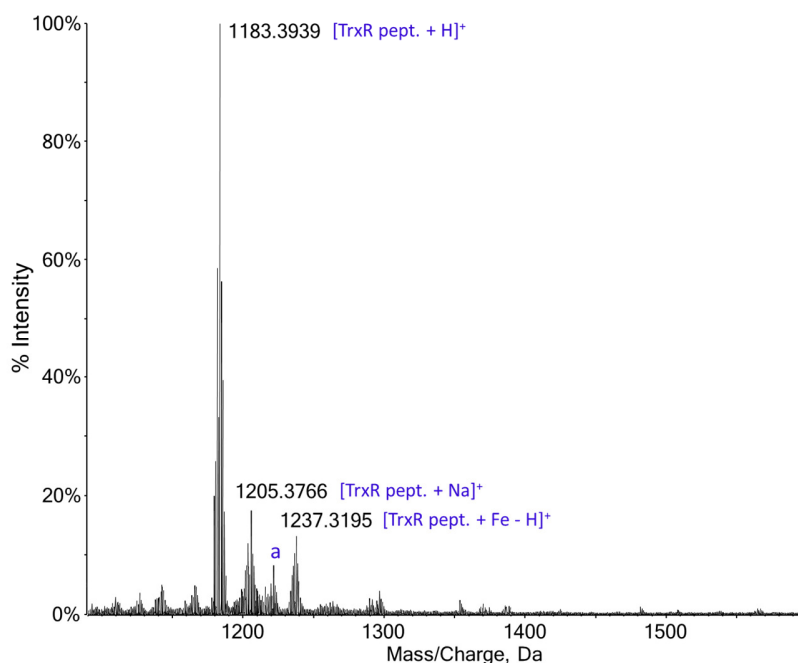


Figure 1. High-resolution ESI mass spectrum of TrxR-pept 10^{-5} M in water and incubated with complex **4b** for 24 hours at 37 °C (1:1 peptide to complex ratio). 0.1% v/v of formic acid was added just before infusion. Unlabelled peak **a** = m/z 1221,4922 corresponds to $[\text{TrxR-pept} + \text{K}]^+$ ion.

3. Partial Least Squares (PLS) Methodology

The bridging vinyliminium ligand in diiron complexes offers a wide opportunity for structural variability by the choice of the substituents R^{1-4} , and indeed more than 100 compounds of this class have been synthesized to date (see Introduction). To assess the effect of R^{1-4} on the biological properties of the complexes, we carried out a multivariate analysis comprising 50 complexes of general formula $[\text{Fe}_2\text{Cp}_2(\text{CO})(\mu\text{-CO})\{\mu\text{-}\eta^1\text{:}\eta^3\text{-C}(\text{R}^4)\text{C}(\text{R}^3)\text{CN}(\text{R}^1)(\text{R}^2)\}]^+$ which have been investigated for their antiproliferative activity (Scheme 1). IC_{50} data for A2780, A2780cisR ovarian cancer cells, Balb/3T3 mouse embryo fibroblasts and HEK-293 human embryonic kidney cells, determined by tetrazolium colorimetric assays (MTT or WST-1) after 72 hours incubation at 37 °C with the diiron compounds, are compiled in Table S1. Since IC_{50} data were collected on different batches of cell lines, cisplatin was taken as reference drug and the *relative cytotoxicity* with respect to cisplatin in the same set of measurements was calculated for each compound/cell line as $\text{Tox} = \text{IC}_{50}(\text{cisplatin}) / \text{IC}_{50}(\text{compound})$.³⁶ Taking Balb/3T3 and HEK-293 as models of non-cancerous lines,³⁷ the *relative cancer cell selectivity* of the compounds was calculated as $\text{Sel} = \text{Tox}(\text{A2780}) / \text{Tox}(\text{non-cancerous cell line})$. Thus, $\text{Tox} > 1$ indicates a higher cytotoxicity as compared to cisplatin, while $\text{Sel} > 1$ indicates an increment in cancer cell selectivity with respect to cisplatin.

Next, ten structural descriptors (**p1-p10** in Table 4) were defined to best describe the variability in R^{1-4} substituents of the bridging vinyliminium ligand; these include the number of aliphatic or aromatic/unsaturated carbons and the number of H-bond donor/acceptor heteroatoms. Wavenumbers of carbonyl and iminium stretching bands and partition coefficients ($\text{Log } P_{\text{ow}}$) of the diiron compounds

were also included in the analysis, to serve both as a check for the structural parametrization and to evaluate the relationship of the latter with biological data.

The chosen structural descriptors have a clear chemical interpretation and are simple to compute. A similar approach was adopted by Österberg and Norinder,³⁸ which correlated the polar surface area of drugs with the number of H-bond acceptor oxygen and nitrogen atoms and the number of hydrogen atoms bonded to these. Differently, the investigation of structure-activity relationship often relies on computational methods to calculate more complex molecular descriptors (*e.g.* orbital energies, molar volume, polarity).³⁹

It is possible that the electronic effects of the various substituents play some minor role by affecting the electrochemical reduction potential of the complexes^{19,40} and thus their ability to produce ROS via the interaction with suitable reducing agents, however these data are not of easy evaluation and have not been included in the present PLS analysis.

As a first step, two separate principal component analyses (PCA) were performed on the complete dataset, for dependent (Log P_{ow} , **Tox** (A2780), **Tox** (A2780cisR), **Sel**) and independent (**p1-p10**) variables. For dependent variables, the first two principal components comprise 92.1 % of the total data variance. Figure S13 shows the biplot of the first two principal components, where it can be easily seen that Log P_{ow} , **Tox** (A2780) and **Tox** (A2780cisR) are positively correlated among each, being at the same time uncorrelated to **Sel**, as indicated by the almost 90° angle between the vectors.

The PCA applied to independent variables (37.3% variance explained by the first two principal components) returns the correlation among the structural and spectroscopic parameters, which can be appreciated in the loading plot reported in Figure S14.

Then we developed three Partial Least Squares (PLS) regression models, correlating the nature of the R¹-R⁴ substituents (**p1-p10**, x variables) with either Log P_{ow} , **Tox** (A2780) or **Sel** (y variable).⁴¹ The regression models were optimized within a fivefold cross validation (CV) scheme (100

randomizations), choosing the most appropriate number of latent variables by looking for the lowest root mean square error of cross validation (RMSECV):

$$RMSECV = \sqrt{\frac{\sum_{i=1}^N (\hat{y}_{CV,i} - y_i)^2}{N}}$$

Where $\hat{y}_{CV,i}$ denotes the predicted y values with CV, y_i is the measured y value, and N is the number of samples. A permutation test (1000 permutations) was also used to validate the obtained models, confirming the statistical significance of the results.

Figure 2 shows the results of the PLS multivariate regression models obtained with the optimal number of latent variables (LVs) for $\text{Log } P_{ow}$. The RMSECV resulted 0.32 with a relevant explained variance of 61.6 %, indicating a satisfactory fit of the training points. RMSECV indicates the standard error associated to prediction of the response in the CV cycles; being expressed with the same measurement units of the response, its numerical value indicates that the prediction error is lower than 20 % of the response range evaluated by the model. Residuals in cross validation, as illustrated in Figure 2d, are randomly distributed, indicating that the postulated linear regression model is suitable for describing the relationship between the structural descriptors and $\text{Log } P_{ow}$. Variables' Importance in the Projection (VIP) column plot (Figure 2f) provides information about the importance of the parameters **p1-p10** in the dataset; $VIP < 1$ indicates a non-important variable from a statistical point of view. Information on the positive or negative effect of each variable is derived from the plot of the coefficients (Figure 2e).

Results show that $\text{Log } P_{ow}$ is positively correlated with the number of unsaturated or aromatic carbons on the iminium (R^1+R^2 , **p2**) and vinyl (R^3 , **p5**) substituents and negatively correlated with the number of H-bond acceptor heteroatoms on the same positions (**p3**, **p6**). These trends agree with the expected contribution of such groups on the lipophilicity.⁴² The lesser impact ($VIP < 1$) of other parameters in describing the distribution of partition coefficients, such as the number of aliphatic carbons or the

number of heteroatoms on R^4 (**p8**, **p10**), can also result from the lower variability explored in the compound dataset (*e.g.* the majority of compounds derive from terminal alkynes, $R^4 = H$).

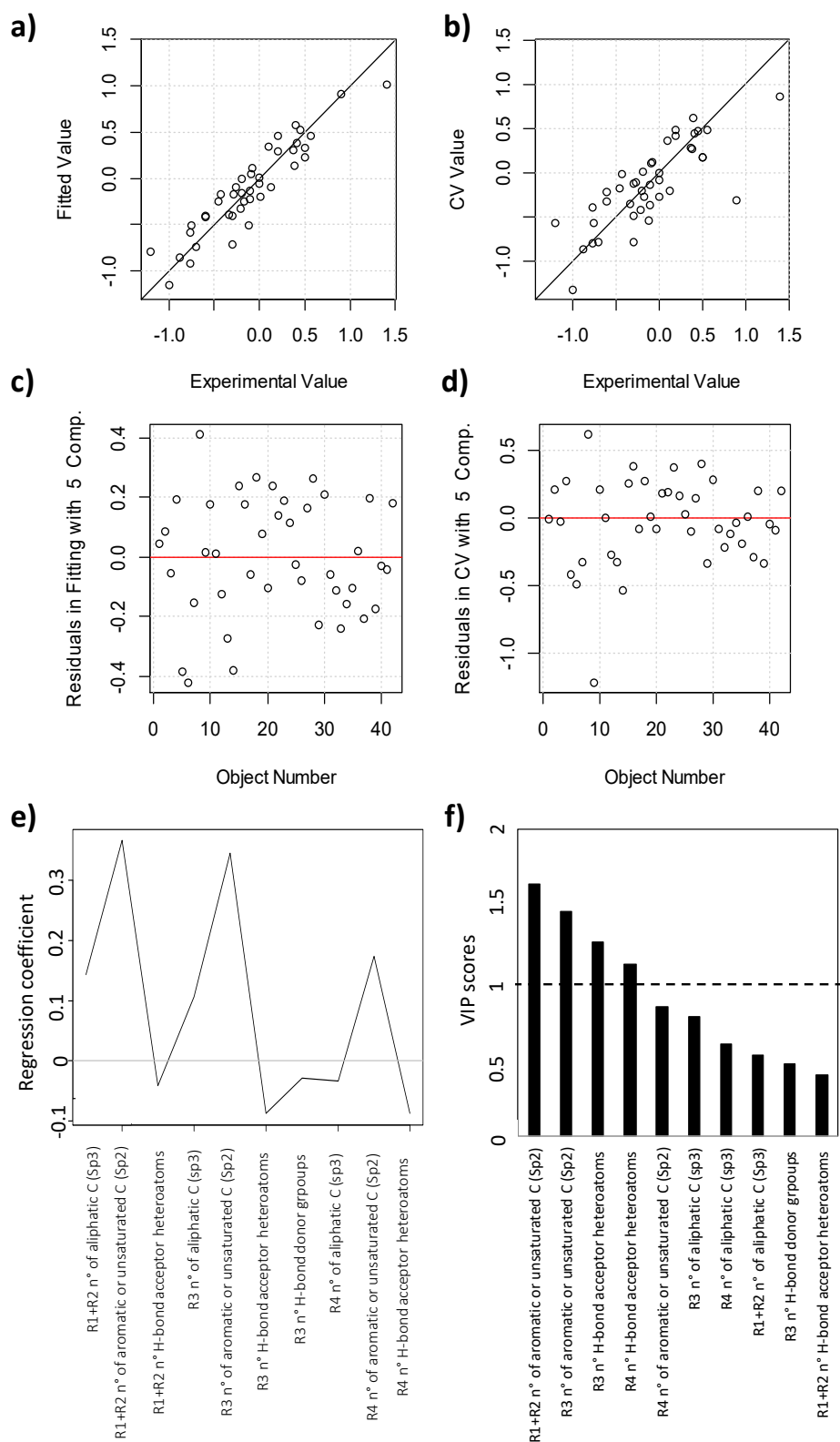


Figure 2. Results of PLS regression model with 5 latent variables for $\text{Log } P_{ow}$: a) Fitted vs. measured scatter plots; b) Predicted in 5-CV vs. measured scatter plots; c) Residuals in fitting; d) Residuals in 5-CV; e) Values of the coefficients for structural parameters **p1-p10**, ordered by decreasing significance; f) VIP plot for **p1-p10**.

Next, we applied the PLS multivariate regression model to **Tox** (A2780) data; results are illustrated in Figure 3. The number of aromatic or unsaturated carbons on R¹, R² and R³ (**p2**, **p5**) are positively correlated with the antiproliferative activity, while a negative correlation is observed for the number of H-bond acceptor heteroatoms on R³ (**p7**). These parameters exert the same effects on Log *P*_{ow}: this in agreement with the PCA, indicating a positive correlation between **Tox** (A2780) and Log *P*_{ow}. Table S2 shows the compounds in order of decreasing cytotoxicity on A2780 cells. For instance, among the 11 compounds that resulted more cytotoxic than cisplatin (**Tox** > 1), 9 possess a xylyl substituent on the iminium group and 7 have an aromatic/heteroaromatic substituent on R³. Besides, with the exception of **4i** and **4l**, the drop of activity upon introduction of heteroatoms on R³, especially oxygenated functions, is evident (*e.g.* compare **4e**, **4g**, **4c**).

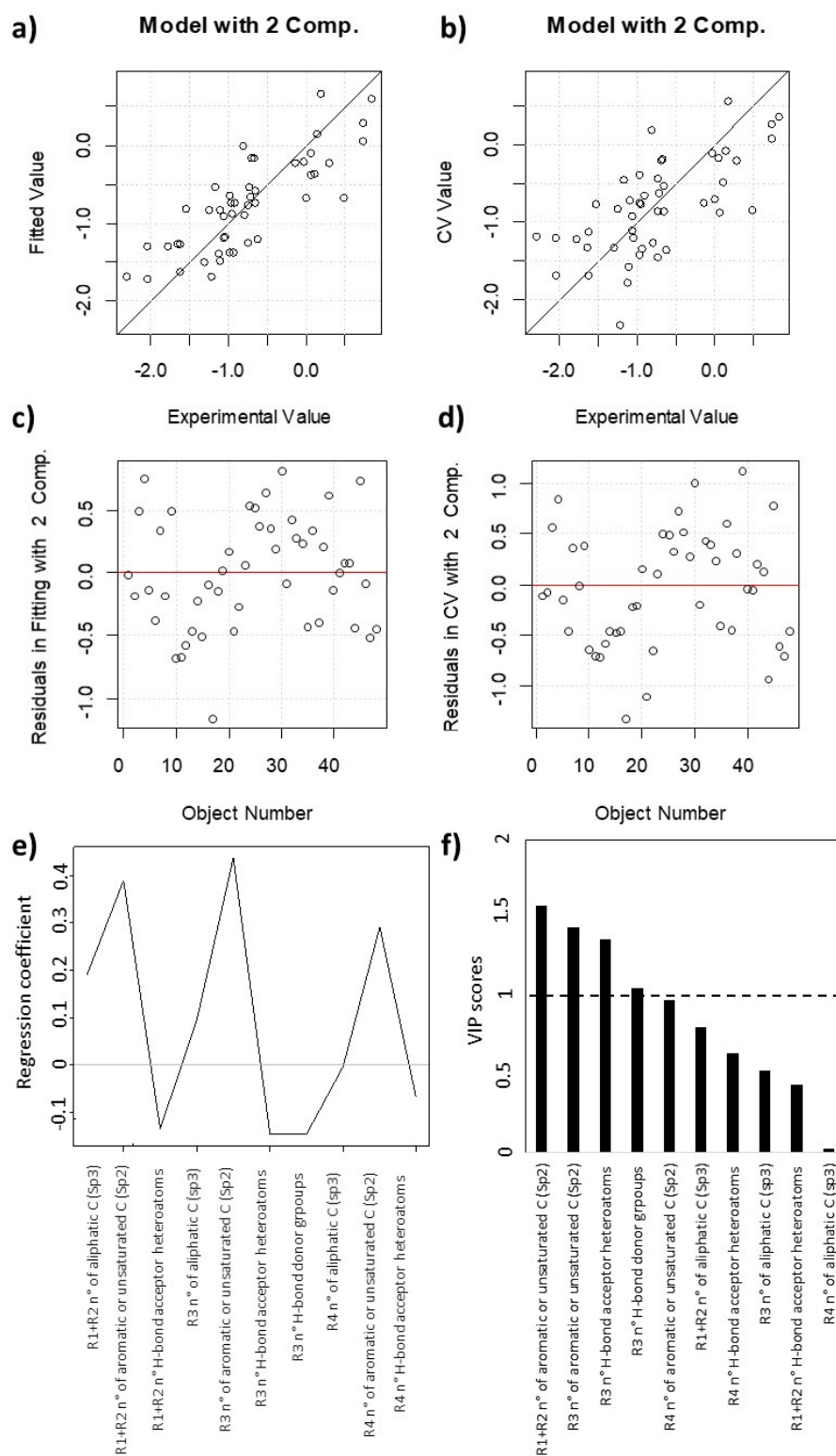


Figure 3. Results of PLS regression model with 2 latent variables for **Tox** (A2780) (RMSECV 0.54, explained variance 45.9%): a) Fitted vs. measured scatter plots; b) Predicted in 5-CV vs. measured scatter plots; c) Residuals in fitting; d) Residuals in 5-CV; e) Values of the coefficients for structural parameters **p1-p10**, ordered by decreasing significance; f) VIP plot for **p1-p10**.

The last PLS regression model was built for the relative cancer cell selectivity **Sel** (Figure 4). In this case, the PLS model performed rather badly (RMSECV 0.53, explained variance 23.1%), which can in part be understood on considering the complexity associated to **Sel** (four IC₅₀ data are involved). The two most important parameters (VIP > 1) are related to R³: the number of aliphatic carbons (**p4**) exerts a positive effect on **Sel** whereas the number of aromatic/unsaturated carbons (**p5**) plays a negative effect. A correlation between the other structural parameters and **Sel** could not be established. Indeed, fourteen out of the eighteen most selective compounds (**Sel** ≥ 4.4), including the first six (**Sel** > 13) possess aliphatic substituents on R³ (Table S2). However, the range of aliphatic groups on R³ has been limitedly explored so far, being confined to Me, Et, SiMe₃ or CO₂Me (the latter also affecting the number of heteroatoms). Conversely, compounds with aryl or heteroaryl groups on R³ rarely outperform cisplatin in terms of cancer cell selectivity (taking **Sel** > 2 as a threshold), with the exception of **4j**, **2m** and **7c**. Note that **p5** plays opposite effects on **Tox** (A2780) and **Sel**, conversely, **p2** and **p4** are only correlated with **Tox** (A2780) and **Sel**, respectively (compare Figures 2f and 3f), thus representing guidelines for the design of new compounds. In other words, an increased cancer cell cytotoxicity could be pursued by introducing aromatic/unsaturated groups on the iminium group (**p2**) while adding aliphatic substituents on R³ should be beneficial for cancer cell selectivity (**p4**). In this regard, the only vinyliminium compound which is at the same time more cytotoxic to A2780 cells (**Tox** > 1) and more selective (**Sel** > 1) than cisplatin is **4b**, bearing a xylyl group on R¹ and a SiMe₃ group on R³.

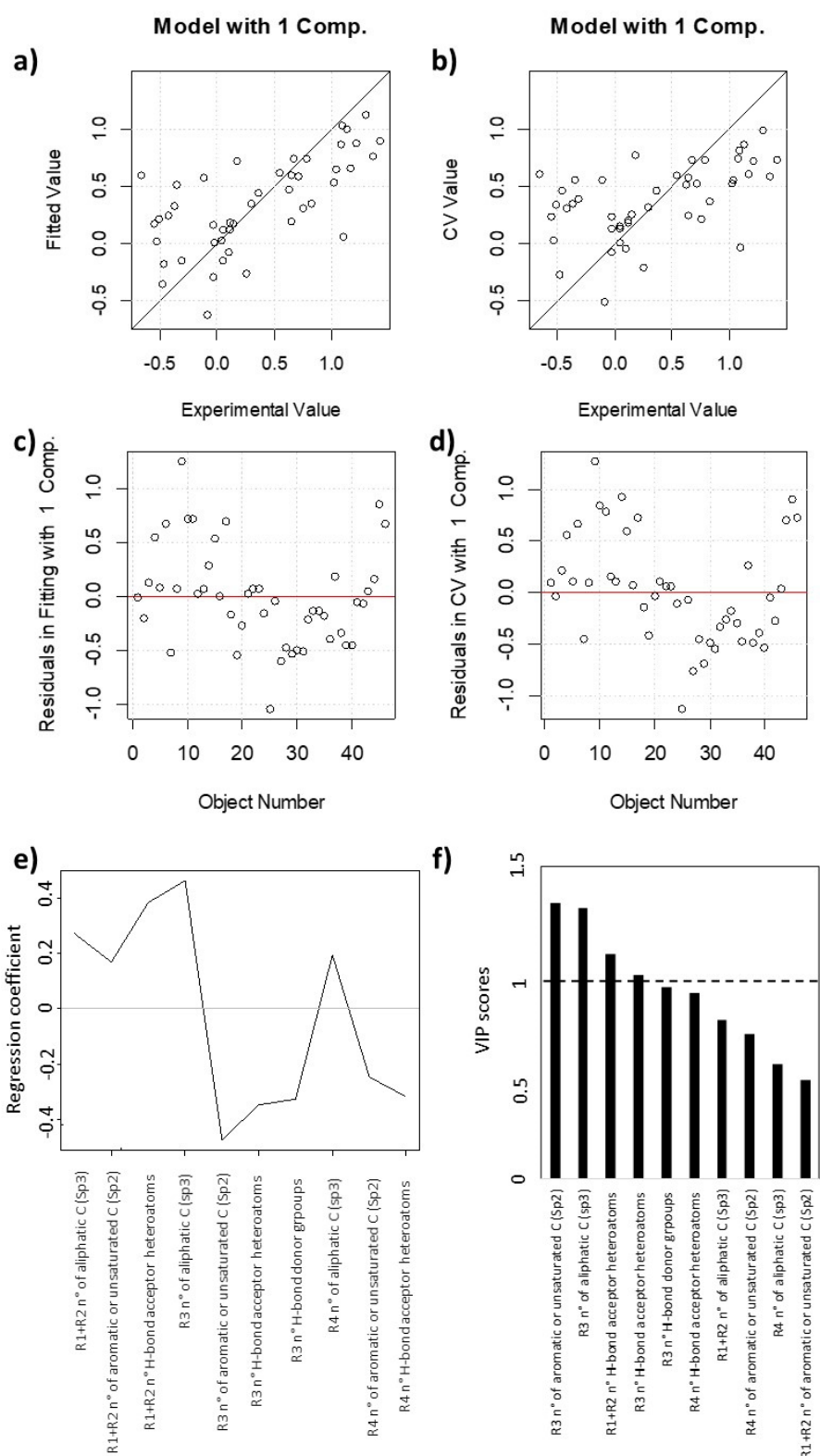


Figure 4. Results of PLS regression model with 1 latent variable for Sel: a) Fitted vs. measured scatter plots; b) Predicted in 5-CV vs. measured scatter plots; c) Residuals in fitting; d) Residuals in 5-CV; e) Values of the coefficients for structural parameters **p1-p10**; f) VIP plot for **p1-p10**.

4. Synthesis of targeted complexes

According to data in Table 2, the trimethylsilyl complex **4b** emerges for its anticancer potential among the newly investigated compounds. Chemometric analysis suggests that the introduction of one aryl group on the iminium moiety (R^1/R^2) together with an alkyl substituent on C^3 (R^3) may represent a convenient choice to enhance the antiproliferative activity of diiron vinyliminium complexes.

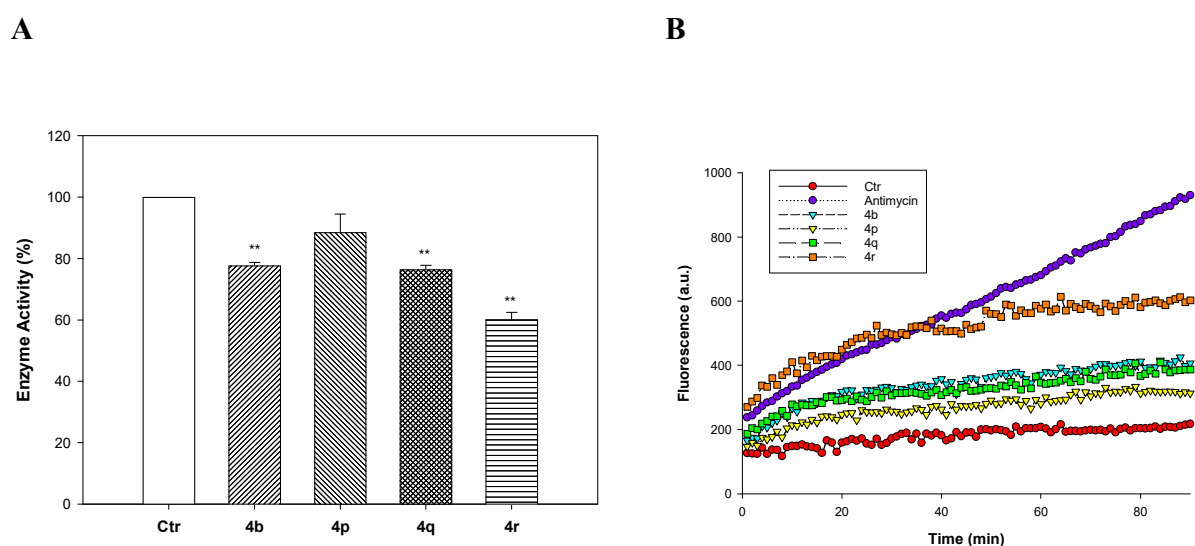
Based on these observations, complexes **4p-r** were synthesized using the procedure shown in Scheme 2, and isolated in 73-83% yields after work-up. The synthesis of **4q** was previously reported,^{13a} while **4p** and **4r** are new, and their spectroscopic characterization is in alignment with general trends (see Experimental for details). The behavior of **4p-r** in aqueous solutions was assessed (Table 1), then these compounds were investigated for their antiproliferative activity against human ovarian A2780 and A2780cisR cancer cell lines. Results reported in Table 3 show that **4p** and **4q** are less effective than **4b** in decreasing cancer cell viability, whereas **4r** displays IC_{50} values in the nanomolar range and is more active than **4b**. Interestingly, the Resistant Factors (R.F., defined as the ratio of the IC_{50} of resistant cells over the IC_{50} of sensitive ones) calculated for complexes **4p-r** are ≤ 1 , thus clearly attesting their ability to overcome cisplatin resistance.

Table 3. IC_{50} values (μM) determined for diiron complexes and cisplatin on human ovarian carcinoma (A2780) and human ovarian carcinoma cisplatin-resistant (A2780cisR) cell lines after 72 hours exposure. Values are given as the mean \pm SD. R.F. = IC_{50} (resistant subline)/ IC_{50} (*wild-type* cells). S.D. = standard deviation.

Complex	A2780	A2780cisR	R.F.
4p	22 \pm 4	11 \pm 2	0.5
4q	5.2 \pm 0.9	3.5 \pm 0.7	0.7
4r	0.2 \pm 0.1	0.2 \pm 0.1	1.0

In addition, we assessed the ability of **4b** and **4p-r** to hamper TrxR activity in A2780 cancer cells. Enzyme activity was measured according to standard procedures described in the Experimental

Section, and results are shown in Figure 5, panel A. All complexes proved to be moderately effective in inhibiting cellular TrxR, consistently with mass analyses performed on **4b** using a model dodecapeptide (see above), and **4r** emerged as the most effective one, being able to inhibit TrxR activity by about 40%. Finally, we evaluated the ability of tested complexes to induce an increase in the cellular basal ROS production. Treatment of A2780 cells with **4b** or **4p-r** determined a time-dependent increase in cellular ROS production (Figure 5, panel B). Remarkably, **4r** elicited an increase in the cellular hydrogen peroxide content similar to that induced by antimycin, a classical inhibitor of the mitochondrial respiratory chain at the level of complex III.



A

Figure 5. Effects on TrxR activity and ROS production. **A:** A2780 cells were incubated for 24 h with the tested compounds (2 μ M). Subsequently, cells were washed twice with PBS and lysed. TrxR activity was tested by measuring NADPH-dependent reduction of DTNB at 412 nm. Error bars indicate SD. * $p < 0.05$, ** $p < 0.01$. **B:** A2780 cells were pre-incubated in PBS/10 mM glucose medium for 20 min at 37 $^{\circ}$ C in the presence of 10 μ M CM-H₂DCFDA and then treated with IC₅₀ concentrations of the tested compounds.

Conclusions

Diiron vinyliminium complexes constitute a hugely populated family of organometallics, and the number of obtainable compounds is theoretically unlimited due to the general character of the synthesis

reaction and the wide availability of organic reagents. The promising anticancer potential of this class of compounds has been recently unveiled, associated with key characteristics which are important prerequisites for a drug candidate. The offered structural variability represents a great arsenal in view of the development of optimal anticancer drugs. Here, we have extended preliminary biological studies to seven complexes not analyzed previously, highlighting that the conjugation of xylyl and trimethylsilyl substituents on the vinyliminium ligand provides a great cytotoxicity effect with respect to that of cisplatin, together with a substantial inertness in aqueous solution and a balanced hydrophilic/lipophilic character. Moreover, by analyzing the biological data collected on almost 50 diiron vinyliminium complexes, we show that simple structural parameters, in combination with PLS statistics, are useful to derive structure-activity relationships, tracing directions for the design of new and more effective drug candidates, avoiding more complex computational approaches. Specifically, results suggest the opportunity to focus future investigations on new compounds containing aromatic/unsaturated groups as iminium substituents while introducing alkyl substituents on the vinyl position. Additional studies confirm the goodness of these concluding remarks, and indeed a new complex with xylyl and pentyl substituents was synthesized and revealed an outstanding cytotoxicity correlated with an enhanced ability to induce ROS production and inhibit Trx-R enzyme.

Experimental

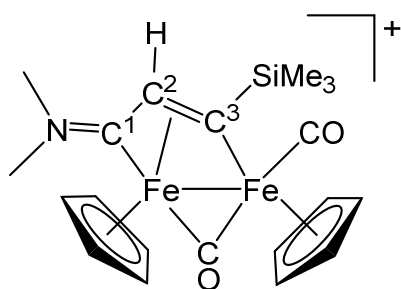
Materials and methods. The preparation and isolation of products were carried out in air. Once isolated, all the products were stored in air. Solvents and organic reactants were purchased from Merck or TCI Europe. Compounds **1a-b**,¹² **2a**,²³ **4a**,²³ and **4d**²⁴ were prepared according to the respective literature procedures. Chromatography separations were carried out on columns of deactivated alumina (Merck, 4% w/w water). Infrared spectra of solutions were recorded on a Perkin Elmer Spectrum 100 FT-IR spectrometer with a CaF₂ liquid transmission cell (2300-1500 cm⁻¹ range). UV-Vis spectra (250-800 nm) were recorded on a Ultraspec 2100 Pro spectrophotometer using PMMA cuvettes (1 cm path length). IR and UV-Vis spectra were processed with Spectragryph software.⁴³ NMR spectra were recorded on a Bruker Avance II DRX400 or Jeol JNM-ECZ400R instruments equipped with broadband probes. Chemical shifts (expressed in parts per million) are referenced to the residual solvent peaks (¹H, ¹³C)⁴⁴ or to external standard (³¹P to 85% H₃PO₄; ²⁹Si to TMS). ¹H and ¹³C NMR spectra were assigned with the assistance of ¹H-¹³C (*gs*-HSQC and *gs*-HMBC) correlation experiments.⁴⁵ NMR signals due to a second isomeric form (where it has been possible to detect them) are italicized. Elemental analyses (CHNS) were performed on a Vario MICRO cube instrument (Elementar).

Synthesis and characterization of diiron vinyliminium complexes. In a typical procedure, diiron aminocarbene complex [**1a-b**]CF₃SO₃ (ca. 0.5 mmol) was dissolved in acetonitrile (10 mL) and treated with Me₃NO (1.3 eq.). The resulting mixture was stirred for 1 hour, and progressive darkening of the solution was observed. The conversion of the starting material into the acetonitrile adduct [Fe₂Cp₂(CO)(μ-CO)(NCMe){μ-CNMe(R)}]CF₃SO₃ (R = Me, Xyl) was checked by IR spectroscopy, as is routine for this type of reaction.⁴⁶ The volatiles were removed under vacuum, thus the residue was dissolved into dichloromethane (ca. 20 mL). The solution was treated with the appropriate alkyne (ca.

1.3 eq.), and the mixture was stirred at room temperature for 48 hours. The final mixture was charged on an alumina column. Elution with CH₂Cl₂ and CH₂Cl₂/THF mixtures allowed the removal of unreacted alkyne and impurities, then a fraction corresponding to the desired product was separated using MeCN or MeOH as eluent. Removal of the solvent under reduced pressure afforded the air-stable product. When using methanol as eluent, the solid was re-dissolved in dichloromethane and this mixture was filtered through a celite pad to remove NaCl from alumina, then the solvent was eliminated under reduced pressure.

[Fe₂Cp₂(CO)(μ-CO){μ-η¹:η³-C³(SiMe₃)C²HC¹NMe₂}]CF₃SO₃, 2b¹³ (Figure 6)

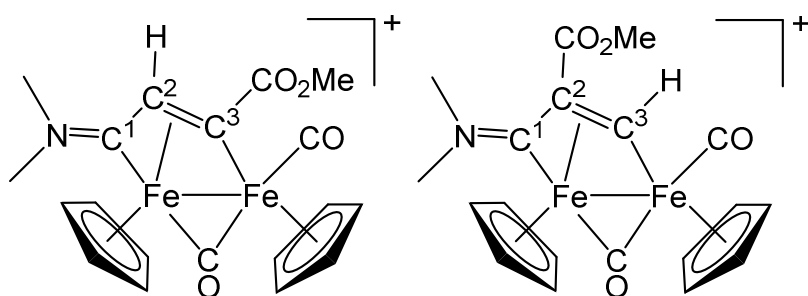
Figure 6. Structure of the cation of **2b**.



From **1a** and trimethylsilylacetylene. Brown solid, yield 90%. Eluent for chromatography: MeCN. Anal. calcd. for C₂₁H₂₆Fe₂F₃NO₅SSi: C, 41.95; H, 4.36; N, 2.33; S, 5.33. Found: C, 41.82; H, 4.52; N, 2.26; S, 5.40. IR (CH₂Cl₂): $\tilde{\nu}/\text{cm}^{-1}$ = 1990vs (CO), 1807s (μ-CO), 1685m (C²C¹N). ¹H NMR (acetone-d₆): δ/ppm = 5.57 (s, 5 H, Cp); 5.22 (s, 5 H, Cp); 4.97 (s, 1 H, C²H); 3.99 (s, 3 H, NMe); 3.35 (s, 3 H, NMe); 0.69 (s, 9 H, SiMe₃). ²⁹Si NMR (acetone-d₆): δ/ppm = 9.36.

[Fe₂Cp₂(CO)(μ-CO){μ-η¹:η³-C³(CO₂Me)C²HC¹NMe₂}]CF₃SO₃, 2c and [Fe₂Cp₂(CO)(μ-CO){μ-η¹:η³-C³HC²(CO₂Me)C¹NMe₂}]CF₃SO₃, 2c'¹⁴ (Figure 7)

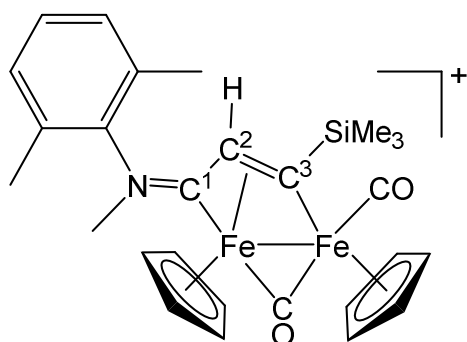
Figure 7. Structure of the cations of **2c** (left) and **2c'** (right).



From **1a** and methyl propiolate. Brown solid, yield 80%. Eluent for chromatography: MeOH. Anal. calcd. for $C_{20}H_{20}F_3Fe_2NO_7S$: C, 40.91; H, 3.43; N, 2.39; S, 5.46. Found: C, 40.76; H, 3.40; N, 2.50; S, 5.50. IR (CH_2Cl_2): $\tilde{\nu}/cm^{-1}$ = 2000vs (CO), 1817s (μ -CO), 1710m (CO_2Me), 1687m (C^2C^1N). **2c**. 1H NMR ($CDCl_3$): δ/ppm = 5.21 (s, 5 H, Cp); 5.15 (s, 5 H, Cp); 4.97 (s, 1 H, C^2H); 4.09 (s, 3 H, OMe); 3.84 (s, 3 H, NMe); 3.29 (s, 3 H, NMe). 1H NMR (acetone- d_6): δ/ppm = 5.46 (s, 5 H, Cp); 5.33 (s, 5 H, Cp); 5.18 (s, 1 H, C^2H); 4.09 (s, 3 H, OMe); 3.97 (s, 3 H, NMe); 3.39 (s, 3 H, NMe). **2c'**. 1H NMR (acetone- d_6): δ/ppm = 12.81 (s, 1H, C^3H); 5.67 (s, 5 H, Cp); 5.11 (s, 5 H, Cp); 4.07 (s, 3 H, OMe); 3.90 (s, 3 H, NMe); 3.39* (NMe). *Superimposed with a signal of **2c**. Isomer ratio (acetone- d_6) = 3:1.

[Fe₂Cp₂(CO)(μ -CO){ μ - η^1 : η^3 -C³(SiMe₃)C²HC¹NMe(Xyl)}]CF₃SO₃, **4b¹³ (Figure 8)**

Figure 8. Structure of the cation of **4b**.

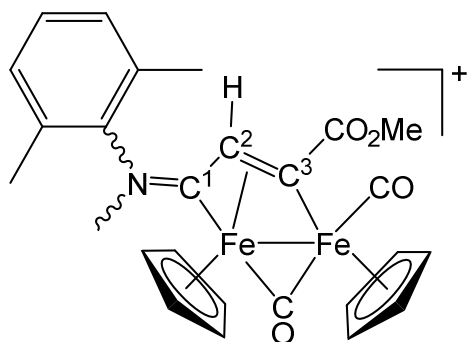


From **1b** and trimethylsilylacetylene. Brown solid, yield 89%. Eluent for chromatography: MeCN. Anal. calcd. for $C_{28}H_{32}F_3Fe_2NO_5SSi$: C, 48.64; H, 4.67; N, 2.03; S, 4.64. Found: C, 48.51; H, 4.76; N,

1.90; S, 4.58. IR (CH₂Cl₂): $\tilde{\nu}/\text{cm}^{-1}$ = 2001vs (CO), 1813s (μ -CO), 1631m (C²C¹N). ¹H NMR (CDCl₃): δ/ppm = 7.21–6.92 (m, 3 H, C₆H₃); 5.44 (s, 5 H, Cp); 5.20 (s, 5 H, Cp); 4.30 (s, 1 H, C²H); 4.25 (s, 3 H, NMe); 2.27 (s, 3 H, C₆H₃Me); 1.77 (s, 3 H, C₆H₃Me); 0.55 (s, 9 H, SiMe₃). ¹H NMR (acetone-d₆): δ/ppm = 7.28–7.17 (m), 7.04 (d, J = 6.6 Hz) (3 H, C₆H₃); 5.73 (s, 5 H, Cp); 5.46 (s, 5 H, Cp); 4.86 (s, 1 H, C²H); 4.52 (s, 1 H, C²H); 4.38 (s, 3 H, NMe); 2.34 (s, 3 H, C₆H₃Me); 1.84 (s, 3 H, C₆H₃Me); 0.61 (s, 9 H, SiMe₃). ²⁹Si NMR (acetone-d₆): δ/ppm = 9.51.

[Fe₂Cp₂(CO)(μ -CO){ μ - η^1 : η^3 -C³(CO₂Me)C²HC¹NMe(Xyl)}]CF₃SO₃, **4c¹⁴ (Figure 9)**

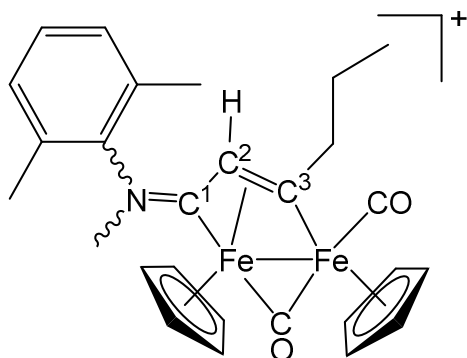
Figure 9. Structure of the cation of **4c**.



From **1b** and methyl propiolate. Brown solid, yield 78%. Eluent for chromatography: MeOH. Anal. calcd. for C₂₇H₂₆F₃Fe₂NO₇S: C, 47.88; H, 3.87; N, 2.07; S, 4.73. Found: C, 47.69; H, 3.92; N, 2.02; S, 4.85. IR (CH₂Cl₂): $\tilde{\nu}/\text{cm}^{-1}$ = 2013vs (CO), 1829s (μ -CO), 1712m (CO₂Me), 1635m (C²C¹N), 1616 w-m (arom C=C). ¹H NMR (CDCl₃): δ/ppm = 7.44–6.92 (m, 3 H, C₆H₃); 5.35, 5.24 (s, 5 H, Cp); 5.34, 4.88 (s, 5 H, Cp); 4.43 (s, 1H, C²H); 4.20, 3.57 (s, 3 H, NMe); 4.16, 4.05 (s, 3 H, OMe); 2.59, 2.29 (s, 3 H, C₆H₃Me); 1.93, 1.73 (s, 3 H, C₆H₃Me). ¹H NMR (acetone-d₆): δ/ppm = 7.51–7.48, 7.38–7.18 (m), 7.07 (d, J = 7.5 Hz) (3 H, C₆H₃); 5.61, 5.57 (s, 5 H, Cp); 5.55, 5.02 (s, 5 H, Cp); 4.89, 4.86 (s, 1 H, C²H); 4.35, 3.68 (s, 3 H, NMe); 4.14, 3.98 (s, 3 H, OMe); 2.59, 2.36 (s, 3 H, C₆H₃Me); 2.01, 1.81 (s, 3 H, C₆H₃Me). *E/Z* ratio = 6 (CDCl₃); 2.6 (acetone-d₆).

[Fe₂Cp₂(CO)(μ-CO){μ-η¹:η³-C³(Pr)C²HC¹NMe(Xyl)}]CF₃SO₃, 4p (Figure 10)

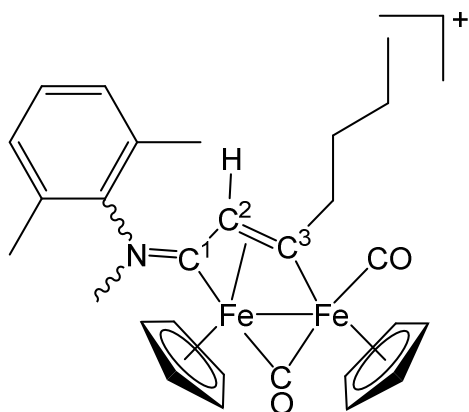
Figure 10. Structure of the cation of 4p.



From **1b** and 1-pentyne. Brown solid, yield 75%. Eluent for chromatography: MeCN/MeOH 9/1. Anal. calcd. for C₂₈H₃₀F₃Fe₂NO₅S: C, 50.85; H, 4.57; N, 2.12; S, 4.85. Found: C, 50.69; H, 4.66; N, 2.06; S, 4.69. IR (CH₂Cl₂): $\tilde{\nu}/\text{cm}^{-1}$ = 2000vs (CO), 1813s (μ -CO), 1712m (CO₂Me), 1634m (C²C¹N). ¹H NMR (acetone-d₆): δ/ppm = 7.25–7.03 (m, 3 H, C₆H₃); 5.65, 5.58 (s, 5 H, Cp); 5.43, 4.91 (s, 5 H, Cp); 4.39, 3.82 (m, 2 H, C³CH₂); 4.34, 3.61 (s, 3 H, NMe); 4.28 (s, 1H, C²H); 2.56, 2.35 (s, 3 H, C₆H₃Me); 2.22, 1.81 (s, 3 H, C₆H₃Me); 2.16–2.09, 1.71–1.62 (m, 2 H, CH₂); 1.10 (t, 3 H, ³J_{HH} = 7.3 Hz, CH₂CH₃). E/Z ratio = 9. ¹³C{¹H} NMR (acetone-d₆): δ/ppm = 255.8 (CO); 234.5 (C¹); 218.2 (C³); 211.5 (CO); 146.1 (ipso-C₆H₃); 132.9, 132.2, 130.3, 130.1, 126.0 (C₆H₃); 92.1, 88.7 (Cp); 57.9 (C³CH₂); 52.0 (C²); 46.4 (NMe); 18.0, 17.3 (C₆H₃Me); 14.4 (C³CH₂CH₃).

[Fe₂Cp₂(CO)(μ-CO){μ-η¹:η³-C³(Bu)C²HC¹NMe(Xyl)}]CF₃SO₃, 4q ^{13a} (Figure 11)

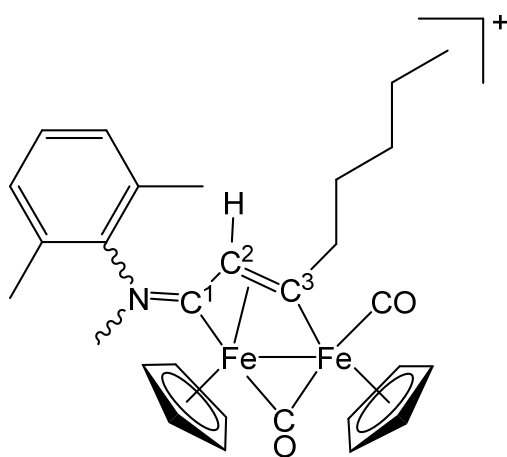
Figure 11. Structure of the cation of 4q.



From **1b** and 1-hexyne. Brown solid, yield 73%. Eluent for chromatography: MeCN/MeOH 9/1. Anal. calcd. for $C_{29}H_{32}F_3Fe_2NO_5S$: C, 51.58; H, 4.78; N, 2.07; S, 4.75. Found: C, 51.42; H, 4.85; N, 1.98; S, 4.82. IR (CH_2Cl_2): $\tilde{\nu}/cm^{-1}$ = 2000vs (CO), 1813s (μ -CO), 1633m (C^2C^1N). 1H NMR (acetone- d_6): δ/ppm = 7.25–6.95 (m, 3 H, C_6H_3); 5.65, 5.59 (s, 5 H, Cp); 5.42, 4.90 (s, 5 H, Cp); 4.48–4.38, 3.87–3.82 (m, 2 H, C^3CH_2); 4.34, 3.61 (s, 3 H, NMe); 4.26 (s, 1H, C^2H); 2.34 (s, 3 H, C_6H_3Me); 1.82 (s, 3 H, C_6H_3Me); 1.68–1.53, 1.28–1.10 (m, 4 H, $C^3CH_2CH_2CH_2CH_3$); 0.98 (t, 3 H, $^3J_{HH} = 7.1$ Hz, $C^3CH_2CH_2CH_2CH_3$). *E/Z* ratio = 8.

[Fe₂Cp₂(CO)(μ -CO){ μ - η^1 : η^3 -C³((CH₂)₄Me)C²HC¹NMe(Xyl)}]CF₃SO₃, **4r (Figure 12)**

Figure 12. Structure of the cation of **4r**.



From **1b** and 1-heptyne. Brown solid, yield 83%. Eluent for chromatography: MeCN/MeOH 9/1. Anal. calcd. for $C_{30}H_{34}F_3Fe_2NO_5S$: C, 52.27; H, 4.97; N, 2.03; S, 4.65. Found: C, 52.38; H, 5.03; N, 1.96; S, 4.57. IR (CH_2Cl_2): $\tilde{\nu}/cm^{-1} = 2002_{vs}$ (CO), 1814_s (μ -CO), 1633_m (C^2C^1N). 1H NMR (acetone- d_6): $\delta/ppm = 7.24-7.02$ (m, 3 H, C_6H_3); 5.64, 5.58 (s, 5 H, Cp); 5.43, 4.90 (s, 5 H, Cp); 4.40, 3.85 (m, 2 H, C^3CH_2); 4.34, 3.60 (s, 3 H, NMe); 4.26 (s, 1H, C^2H); 2.56, 2.34 (s, 3 H, C_6H_3Me); 2.01, 1.81 (s, 3 H, C_6H_3Me); 1.76-1.28 (m, 6 H, $C^3CH_2CH_2CH_2CH_2CH_3$); 0.88 (t, 3 H, $^3J_{HH} = 7.3$ Hz, CH_2CH_3). *E/Z* ratio = 9. $^{13}C\{^1H\}$ NMR (acetone- d_6): $\delta/ppm = 255.8$ (CO); 234.5 (C^1); 218.6 (C^3); 211.5 (CO); 146.1 (ipso- C_6H_3); 132.9, 132.2, 130.3, 130.1 (C_6H_3); 92.1, 88.7 (Cp); 55.9 (C^3CH_2); 51.9 (C^2); 46.4 (NMe); 36.2 ($C^3CH_2CH_2$); 32.7 ($C^3CH_2CH_2CH_2$); 23.2 ($C^3CH_2CH_2CH_2CH_2$); 18.1, 17.4 (C_6H_3Me); 14.4 ($C^3CH_2CH_2CH_2CH_2CH_3$).

Solubility in D_2O . A suspension of the selected iron compound (*ca.* 3 mg) in a D_2O solution (0.3 mL) containing dimethylsulphone (Me_2SO_2) as internal standard⁴⁷ ($3.28 \cdot 10^{-3}$ M) was vigorously stirred at room temperature (*ca.* 21 °C) for 2 h. The resulting saturated solution was filtered over celite, transferred into an NMR tube, diluted with D_2O up to 0.6 mL, and analyzed by 1H NMR (delay time = 3 s; number of scans = 20). The concentration of the saturated solution (solubility) was calculated by the relative integral with respect to Me_2SO_2 ($\delta/ppm = 3.16$ (s, 6H)). Results are compiled in Table 1.

Octanol/water partition coefficient (Log P_{ow}). Partition coefficients (P_{ow} ; IUPAC: K_D partition constant⁴⁸), defined as $P_{ow} = c_{org}/c_{aq}$, where c_{org} and c_{aq} are molar concentrations of the selected compound in the organic and aqueous phase, respectively, were determined by the shake-flask method and UV-Vis measurements.^{32,49} Deionized water and 1-octanol were vigorously stirred for 24 h, to allow saturation of both phases. A stock solution of the iron compound (**4a-d** and **4p-r**, *ca.* 2 mg) was prepared by first adding acetone (50 μ L, to assist solubilization), followed by water-saturated octanol

(3.0 mL). The solution was diluted with water-saturated octanol (*ca.* 1:3 *v/v* ratio, $c_{\text{Fe}2} \approx 10^{-4}$ M, so that $1.5 \leq A \leq 2.0$ at 340 nm) and its UV-Vis spectrum was recorded (A_{org}^0). An aliquot of the solution ($V_{\text{org}} = 1.2$ mL) was transferred into a test tube and octanol-saturated water ($V_{\text{org}} = V_{\text{aq}} = 1.2$ mL) was added. The mixture was vigorously stirred for 30 min at room temperature (*ca.* 21 °C) then centrifuged (5000 rpm, 5 min). The UV-Vis spectrum of the organic phase was recorded (A_{org}^f) and the partition coefficient was calculated as $P_{\text{ow}} = A_{\text{org}}^f / (A_{\text{org}}^0 - A_{\text{org}}^f)$ where A_{org}^0 and A_{org}^f are the absorbance in the organic phase before and after partition with the aqueous phase, respectively.^{49c} The partition coefficient was calculated as $P_{\text{ow}} = (A_{\text{aq}}^0 - A_{\text{aq}}^f) / A_{\text{aq}}^f$ where A_{aq}^0 and A_{aq}^f are the absorbance in the aqueous phase before and after partition with the organic phase, respectively. The absorbance at 340 nm (shoulder band) was used for quantitation. For compounds **2a-c** an inverse procedure was adopted, starting from an aqueous stock solution. The procedure was repeated three times for each sample (from the same stock solution); results are given as mean \pm standard deviation (Table 1).

Stability in D₂O/DMSO-d₆ solution at 37 °C.

The selected iron compound (*ca.* 3-4 mg) was dissolved in DMSO-d₆ (0.1 mL) then diluted with a D₂O solution containing Me₂SO₂ ($3.28 \cdot 10^{-3}$ M; 0.6 mL); a different ratio (0.2/0.5 mL) was used for **4a** and **4p-r**. The mixture was stirred for 30 min then filtered over celite and transferred into an NMR tube. The orange-brown solution ($c_{\text{Fe}} = 8 \cdot 10^{-3}$ M) was analyzed by ¹H NMR (delay time = 3 s; number of scans = 20) then heated at 37 °C for 48 h. After cooling to room temperature, the final solution was separated from a brown solid by filtration over celite and the ¹H NMR spectrum was recorded. In each case, no new {FeCp} species was identified. The residual amount of starting material in solution (% with respect to the initial spectrum) was calculated by the relative integral with respect to Me₂SO₂ as internal standard⁴⁷ (Table 1). ¹H NMR signals and isomer ratios for the tested compounds are reported below; chemical shifts are referenced to Me₂SO₂ peak as in pure D₂O [$\delta/\text{ppm} = 3.16$ (s, 6H)].

2a. ^1H NMR ($\text{D}_2\text{O}:\text{DMSO-d}_6$ 6:1 v/v): $\delta/\text{ppm} = 12.28$ (d, $J = 7.1$ Hz, 1 H, C^3H); 5.42 (s, 5 H), 5.08 (s, 5 H) (Cp); 4.93 (d, $J = 7.1$ Hz, 1 H, C^2H); 3.82 (s, 3 H), 3.27 (s, 3 H) (NMe_2).

2b. ^1H NMR ($\text{D}_2\text{O}:\text{DMSO-d}_6$ 6:1 v/v): $\delta/\text{ppm} = 5.48$ (s, 5 H), 5.11 (s, 5 H) (Cp); 4.89 (s, 1 H, C^2H); 3.86 (s, 3H), 3.25 (s, 3H) (NMe_2); 0.67 (s, 9 H, SiMe_3).

2c. ^1H NMR ($\text{D}_2\text{O}:\text{DMSO-d}_6$ 6:1 v/v): $\delta/\text{ppm} = 5.38$ (s, 5 H), 5.24 (s, 5 H) (Cp); 5.05 (s, 1H, C^2H); 4.15 (s, 3 H) (CO_2Me); 3.84 (s, 3 H), 3.29 (s, 3H) (NMe_2). **2c'.** ^1H NMR ($\text{D}_2\text{O}:\text{DMSO-d}_6$ 6:1 v/v): $\delta/\text{ppm} = 12.79$ (s, 1 H, C^3H); 5.53 (s, 5 H), 5.09 (s, 5 H) (Cp); 3.94 (s, 3 H), 3.93 (s, 3 H), 2.73 (s, 3 H) ($\text{NMe}_2 + \text{OMe}$). Isomer ratio (**2c/2c'**) = 4.3 (0-48 h).

4a. ^1H NMR ($\text{D}_2\text{O}:\text{DMSO-d}_6$ 6:1 v/v): $\delta/\text{ppm} = 12.60$, 12.35 (d, $J = 7.1$ Hz, 1H, C^3H); 7.33–7.24, 7.13–7.05 (m, 3 H) (C_6H_3); 5.55, 5.50 (s, 5 H), 5.26* (s, 3.5 H) (Cp); 5.29, 4.71 (d, $J = 7.1$ Hz, 1 H, C^2H); 4.21, 3.57 (s, 3 H, NMe); 2.51, 2.30 (s, 3H), 1.97, 1.79 (s, 3 H) ($\text{C}_6\text{H}_3\text{Me}_2$). Isomer (E/Z) ratio = 2.6 (0 h); 2.3 (48 h). *Other Cp hidden by HDO peak.

4b. ^1H NMR ($\text{D}_2\text{O}:\text{DMSO-d}_6$ 5:2 v/v): $\delta/\text{ppm} = 7.33$ –7.23 (m, 2 H), 7.09 (d, $J = 6.7$ Hz, 1 H) (C_6H_3); 5.63, 5.54 (s, 5 H), 5.33, 5.24 (s, 5 H) (Cp); 4.41 (s, 1 H, C^2H); 4.27 (s, 3 H, NMe); 2.29 (s, 3 H), 1.84 (s, 3 H) ($\text{C}_6\text{H}_3\text{Me}_2$), 0.73, 0.59 (s, 9 H, SiMe_3). Isomer (E/Z) ratio = *ca.* 12 (0 h); 8.5 (48 h) .

4c. ^1H NMR ($\text{D}_2\text{O}:\text{DMSO-d}_6$ 6:1 v/v): $\delta/\text{ppm} = 7.55$ –7.50, 7.40–7.23, 7.09 (d, $J = 6.8$ Hz) (3 H, C_6H_3); 5.50, 5.45 (s, 5 H), 5.43, 4.96 (s, 5 H) (Cp); 4.23, 3.59 (s, 3 H, NMe); 4.20, 4.06 (s, 3 H, OMe); 2.51, 2.28 (s, 3 H), 1.99, 1.80 (s, 3 H) ($\text{C}_6\text{H}_3\text{Me}_2$). Isomer (E/Z) ratio = 2.0 (0 h); 1.3 (48 h).

4d. ^1H NMR ($\text{D}_2\text{O}:\text{DMSO-d}_6$ 6:1 v/v): $\delta/\text{ppm} = 7.54$ –7.45, 7.31–7.23, 7.07 (d, $J = 7.0$ Hz) (3 H, C_6H_3); 5.53, 5.46 (s, 5 H), 5.26, 4.92 (s, 5 H) (Cp); 4.30–4.24, 3.84–3.75 (m, 2 H, $\underline{\text{CH}_2\text{CH}_3}$); 4.23, 3.53 (s, 3 H, NMe); 4.14 (s, 1 H, C^2H); 2.49, 2.28 (s, 3 H), 2.01, 1.81 (s, 3 H) ($\text{C}_6\text{H}_3\text{Me}_2$); 1.48, 1.30 (t, $J = 7.1$ Hz, 3H, $\underline{\text{CH}_2\text{CH}_3}$). Isomer (E/Z) ratio = 7.6 (0 h); 6.0 (48 h).

4p. ^1H NMR ($\text{D}_2\text{O}:\text{DMSO-d}_6$ 5:2 v/v): $\delta/\text{ppm} = 7.36$ –7.29, 7.14–7.12 (m, 3 H, C_6H_3); 5.58, 5.51 (s, 5 H), 5.32, 4.87 (s, 5 H) (Cp); 4.32, 3.77–3.68 (m, 2 H, C^3CH_2); 4.27 (s, 3 H, NMe); 4.14 (s, 1H, C^2H);

2.32 (s, 3 H, C₆H₃Me); 2.17-2.07, 1.74-1.65 (m, 2 H, CH₂); 1.85 (s, 3 H, C₆H₃Me); 1.15 (t, 3 H, ³J_{HH} = 7.4 Hz, C³CH₂CH₃). Isomer (*E/Z*) ratio = *ca.* 30 (0 h); *ca.* 12 (48 h).

4q. ¹H NMR (D₂O:DMSO-d₆ 5:2 *v/v*): δ/ppm = 7.38–7.31, 7.14 (m, 3 H, C₆H₃); 5.59, 5.52 (s, 5 H, Cp); 5.34, 4.88 (s, 5 H, Cp); 4.37-4.32, 3.84-3.74 (m, 2 H, C³CH₂); 4.28 (s, 3 H, NMe); 4.13 (s, 1H, C²H); 2.34 (s, 3 H, C₆H₃Me); 2.06, 1.64 (m, 4 H, C³CH₂CH₂CH₂CH₃); 1.87 (s, 3 H, C₆H₃Me); 1.08 (t, 3 H, ³J_{HH} = 7.1 Hz, C³CH₂CH₂CH₂CH₃). Isomer (*E/Z*) ratio = *ca.* 9 (0 h); *ca.* 7 (48 h).

4r. ¹H NMR (D₂O:DMSO-d₆ 5:2 *v/v*): δ/ppm = 7.37–7.30, 7.13 (m, 3 H, C₆H₃); 5.58, 5.52 (s, 5 H, Cp); 5.33, 5.01 (s, 5 H, Cp); 4.37-4.31, 3.81-3.74 (m, 2 H, C³CH₂); 4.27 (s, 3 H, NMe); 4.10 (s, 1H, C²H); 2.33 (s, 3 H, C₆H₃Me); 2.14-2.04, 1.73-1.64 1.76-1.28 (m, 2 H, C³CH₂CH₂); 1.86 (s, 3 H, C₆H₃Me); 1.59-1.37 (m, 4 H, C³CH₂CH₂CH₂CH₂CH₃); 0.94 (t, 3 H, ³J_{HH} = 7.1 Hz, CH₂CH₃). Isomer (*E/Z*) ratio = *ca.* 38 (0 h); *ca.* 30 (48 h).

Cell culture and cytotoxicity studies.

In vitro cytotoxicity investigations were carried out by using human ovarian carcinoma cisplatin-sensitive A2780 (ECACC93112519), human ovarian carcinoma cisplatin-resistant A2780cisR (ECACC 93112517) and mouse embryo fibroblasts Balb/3T3 clone A31 (ATCC CCL-163) cell lines. A2780 and A2780cisR were purchased from the European Collection of Authenticated Cell Cultures (ECACC), and Balb/3T3 clone A31 cell line from the American Type Culture Collection (ATCC).

A2780 and A2780cisR cells were routinely cultured in RPMI 1640 (Merck) containing 2 mM of L-glutamine (Merck), 1% of penicillin/streptomycin solution (Merck—10 000 U mL⁻¹: 10 mg mL⁻¹), 10% of foetal bovine serum (Merck—FBS) and antimycotic (InvivoGen, USA), and Balb/3T3 clone A31 in Dulbecco's modified Eagle medium (Merck—DMEM) supplemented with 4 mM of L-glutamine, 1% of penicillin/streptomycin solution, 10% of calf serum (Merck) and antimycotic. The

acquired resistance of A2780cisR cells was maintained by routine supplementation of media with 1 μM of cisplatin (Merck). The cultures were maintained at 37 °C and in a 5% CO₂-enriched atmosphere.

The WST-1 assay was conducted for cell viability investigation. A2780, A2780cisR cells and Balb/3T3 clone A31 cells were seeded in 96-well plates at a final concentration of 3×10^3 , 6×10^3 and 1×10^3 cells per well, respectively. After overnight incubation, the cells were treated with different concentrations (0–100 μM) of the selected compounds. Stock solutions of compounds were prepared in DMSO and sequentially diluted in medium (final DMSO concentration of 0.5%). Cells incubated with cisplatin (0–100 μM) were used as positive control. After 72 hours at 37 °C and in a 5% CO₂-enriched atmosphere, cells were incubated for 4 hours with the WST-1 tetrazolium salt reagent (Roche) diluted 1:10, at 37 °C and 5% CO₂. Measurements of formazan dye absorbance, which directly correlates with the number of viable cells, were carried out with a micro-plate reader (Biorad) at 450 nm, using 655 nm as reference wavelength. The 50% inhibitory concentration (IC₅₀) refers to compound concentration at which 50% of cell death is observed with respect to the control. For each tested compound, assay was performed on triplicate. The concentration effect curves were generated by nonlinear regression curves (GraphPad Prism Software) and the data reported as mean \pm standard deviation.

Interaction with biomolecules.

Stock solutions of TrxR-pept and Cyt c 10^{-3} M were prepared, dissolving the lyophilized peptide and protein and the peptide in LC-MS grade water. The stock solution 10^{-2} M of **4b** was prepared by dissolving the sample in DMSO. For the experiments with **TrxR-pept**, a solution of the peptide 10^{-4} M was prepared by diluting the previous stock solution with LC-MS grade water. Afterwards, a suitable aliquot of the diiron compound solution was added in 1:1 peptide-to-metal compound ratio. The mixture thus obtained was incubated at 37 °C for 24 h. The solution was diluted to a final protein concentration of 10^{-7} M with LC-MS grade water and 0.1% v/v of formic acid was added just before

infusion into the mass spectrometer. For the experiments with Cyt c, a solution of the protein 10^{-4} M and compound **4b** was prepared at protein-to-metal ratios 1:2 by diluting with ammonium acetate solution 2×10^{-3} M (pH 6.8) the respective stock solutions. The mixture was then incubated at 37 °C for 24 h. The solution was diluted to a final protein concentration of 10^{-7} M with ammonium acetate solution 2×10^{-3} M (pH 6.8) and 0.1% v/v of formic acid was added just before infusion into the mass spectrometer. The ESI mass spectra were acquired using a TripleTOF[®] 5600⁺ high-resolution mass spectrometer (Sciex, Framingham, MA, U.S.A.), equipped with a DuoSpray[®] interface operating with an ESI probe. All the ESI mass spectra were acquired through direct infusion at 5 μ L/min flow rate. The general ESI source parameters were optimized as follows:

TrxR-pept: positive polarity, ionspray voltage floating (ISFV) 5500 V, temperature (TEM) 25 °C, ion source gas 1 (GS1) 25 L/min; ion source gas 2 (GS2) 0 L/min; curtain gas (CUR) 30 L/min, collision energy (CE) 10 V; declustering potential (DP) 300 V, acquisition range 1090-2000 *m/z*.

Cyt c: positive polarity, ionspray voltage floating (ISFV) 5500 V, temperature (TEM) 25 °C, ion source gas 1 (GS1) 35 L/min; ion source gas 2 (GS2) 0 L/min; curtain gas (CUR) 20 L/min, declustering potential (DP) 180 V, collision energy (CE) 10 V, acquisition range 500–1800 *m/z*.

For acquisition, Analyst TF software 1.7.1 (Sciex) was used and deconvoluted spectra were obtained by using the Bio Tool Kit micro-application v.2.2 embedded in PeakView[™] software v.2.2 (Sciex).

Data analysis.

Compound selection and data treatment. Diiron vinyliminium compounds of general formula $[\text{Fe}_2\text{Cp}_2(\text{CO})(\mu\text{-CO})\{\mu\text{-}\eta^1\text{:}\eta^3\text{-C}(\text{R}^4)\text{C}(\text{R}^3)\text{CN}(\text{R}^1)(\text{R}^2)\}]^+$ (as CF_3SO_3^- salts, except where otherwise noted) analyzed in this manuscript or in previous publications for cytotoxicity on A2780, A2780cisR, HEK-293 and Balb/3T3 cells were included in this study.^{15,16,18,19,20} Compounds conjugated with specific bioactive fragments (*e.g.* carbohydrates, ferrocenyl, enzyme inhibitors) were excluded.^{17,18} IC₅₀

data, measured after 72 hours incubation, octanol-water partition coefficients ($\text{Log } P_{\text{ow}}$) and wavenumbers of carbonyl and iminium stretching of selected compounds are compiled in Table S1.

Then, IC_{50} data were normalized by defining new parameters as follows:

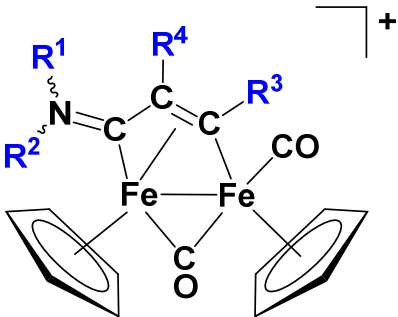
i) $\text{Tox} = \text{IC}_{50}(\text{cisplatin}) / \text{IC}_{50}(\text{compound})$, express the relative toxicity for a selected cell line as compared to cisplatin, measured under equal conditions; $\text{Tox} > 1$: more cytotoxic than cisplatin; $\text{Tox} < 1$: less cytotoxic than cisplatin.

ii) $\text{Sel} = \text{Tox}(\text{A2780}) / \text{Tox}(\text{non-cancerous cell line})$ express the increment in cancer cell selectivity as compared to cisplatin, measured under equal conditions; $\text{Sel} > 1$: more selective than cisplatin; $\text{Sel} < 1$: less selective than cisplatin.

For the sake of this calculation, standard deviation of IC_{50} and $\text{Log } P_{\text{ow}}$ data was not considered. $\text{IC}_{50} > 200 \mu\text{M}$ was considered as $350 \mu\text{M}$; $\text{IC}_{50} > 100 \mu\text{M}$ was considered as $150 \mu\text{M}$. Sel was not calculated for **2h** and **2p**, having undefined IC_{50} ($> 200 \mu\text{M}$) on both A2780 and HEK-293 cells. Data are compiled in Table S2.

Structural parametrization. Ten structural descriptors for R^1 - R^4 substituents were defined as follows (**p1-p10**; Table 4). Stereochemical considerations (*e.g.* *ortho/meta/para* substitution) were discarded.

Table 4. Structural parameters for diiron vinyliminium complexes.

p1	n° of aliphatic (sp^3) carbons on $\text{R}^1 + \text{R}^2$	
p2	n° of aromatic or unsaturated (sp^2) carbons on $\text{R}^1 + \text{R}^2$	
p3	n° of <i>H</i> -bond acceptor heteroatoms ^[a] on $\text{R}^1 + \text{R}^2$	
p4	n° of aliphatic (sp^3) carbons ^{[b][c]} on R^3	
p5	n° of aromatic or unsaturated (sp^2) carbons on R^3	
p6	n° of <i>H</i> -bond acceptor heteroatoms ^[a] on R^3	
p7	n° of <i>H</i> -bond donor groups ^[d] on R^3	
p8	n° of aliphatic (sp^3) carbons ^[c] on R^4	
p9	n° of aromatic or unsaturated (sp^2) carbons on R^4	
p10	n° of <i>H</i> -bond acceptor heteroatoms ^[a] on R^4	

[a] O, N, F, S, Se. [b] -SiMe₃ counted as -CMe₃. [c] Hydrogen substituent is counted as -1. [d] OH = 1; NH₂ = 2; these are also counted as H-bond acceptor heteroatoms.

Chemometric analysis. Since **Tox** (A2780) and **Sel** data were not normally distributed, Log₁₀ transformation was applied to both responses. Moreover, all data were mean centered and unit variance scaled. For the PLS data treatment, the R-based chemometric freeware CAT (Chemometric Agile Tool) developed by the Group of Chemometrics of the Italian Chemical Society was used (<http://gruppochemiometria.it/index.php/software>).

TrxR Inhibition

A2780 cells were grown in 75 cm² flasks at confluence and treated with tested complexes at concentrations corresponding to IC₅₀ values for 24 h. At the end of incubation time, cells were collected, washed with ice cold PBS and centrifuged at 300xg. Each sample was then lysed with RIPA buffer modified as follows: 150 mM NaCl, 50 mM Tris-HCl, 1% Triton X-100, 1% SDS, 1% DOC, 1 mM NaF, 1 mM EDTA, and immediately before use, an anti-protease cocktail (Roche, Basel, Switzerland) containing PMSF was added. Samples were tested for TrxR activity as above described.

Reactive Oxygen Species (ROS) production

The production of ROS was measured in A2780 cells (10⁴ per well) grown for 24 h in a 96-well plate in RPMI medium without phenol red (Sigma Chemical Co.). Cells were then washed with ice cold PBS and loaded with 10 μM 5-(and-6)-chloromethyl-2',7'-dichlorodihydrofluorescein diacetate acetyl ester (CM-H₂DCFDA) (Molecular Probes-Invitrogen, Eugene, OR) for 25 min, in the dark. Afterwards, cells were washed with PBS and incubated with tested compounds. Fluorescence increase was estimated utilizing the wavelengths of 485 nm (excitation) and 527 nm (emission) in an Infinite® 200

PRO (Tecan, Switzerland) plate reader. Antimycin (3 μ M, Sigma Chemical Co), a potent inhibitor of Complex III in the electron transport chain was used as positive control.

Acknowledgements

The University of Pisa is acknowledged for funding (PRA_2020_39).

Supporting Information Available

^1H , ^{13}C and ^{29}Si NMR spectra; ESI mass spectrum for the Cyt c/4b interaction; collection of cytotoxicity, lipophilicity and infrared data; principal component analyses.

References

- (a) E. J. Anthony, E. M. Bolitho, H. E. Bridgewater, O. W. L. Carter, J. M. Donnelly, C. Imberti, E. C. Lant, F. Lermyte, R. J. Needham, M. Palau, P. J. Sadler, H. Shi, F.-X. Wang, W.-Y. Zhang, Z. Zhang, Metallodrugs are unique: opportunities and challenges of discovery and development. *Chem. Sci.*, 2020, 11, 12888–12917. (b) M. Marloye, G. Berger, M. Gelbcke, A survey of the mechanisms of action of anticancer transition metal complexes. *Future Med. Chem.* 2016, 8, 2263-2286. (c) E. Boros, P. J. Dyson, G. Gasser, Classification of Metal-Based Drugs according to Their Mechanisms of Action. *Chem* 2020, 6, 41–60. (d) K. L. Haas, K. J. Franz. Application of Metal Coordination Chemistry To Explore and Manipulate Cell Biology. *Chem. Rev.* 2009, 109, 4921–4960.
- (a) Y.-C. Liu, J. J. Miller, Platinum-Based Anticancer Drugs. *Encyclopedia of Inorganic and Bioinorganic Chemistry* 2020, eibc0178.pub2. (b) S. Ghosh, Cisplatin: The first metal based anticancer drug. *Bioorg. Chem.* 2019, 88, 102925. (c) I. A. Riddell, S. J. Lippard, Cisplatin and Oxaliplatin: Our Current Understanding of Their Actions, *Met. Ions Life Sci.* 2018, 18, 1–42.
- (a) B. S. Murray, P. J. Dyson, Recent progress in the development of organometallics for the treatment of cancer. *Curr. Opin. Chem. Biol.*, 2020, 56, 28-34. (b) P. Štarha, Z. Trávníček, Non-platinum complexes containing releasable biologically active ligands. *Coord. Chem. Rev.*, 2019, 395, 130-145. (c) I. Bratsos, T. Gianferrara, E. Alessio, C. G. Hartinger, M. A. Jakupec, B. K. Keppler, Ruthenium and Other Non-Platinum Anticancer Compounds, in *Bioinorganic Medicinal Chemistry*, ed. E. Alessio, Wiley-VCH,

-
- Weinheim, 2011, 151-174. (d) Ong, Y. C.; Gasser, G. Organometallic compounds in drug discovery: Past, present and future. *Drug Discovery Today* 2020, 37, 117-124.
- 4 Selected references: (a) S. M. Meier-Menches, C. Gerner, W. Berger, C. G. Hartinger, B. K. Keppler, Structure-activity relationships for ruthenium and osmium anticancer agents - towards clinical development. *Chem. Soc. Rev.* 2018, 47, 909-928. (b) R. G. Kenny, C. J. Marmion, Toward Multi-Targeted Platinum and Ruthenium Drugs-A New Paradigm in Cancer Drug Treatment Regimens? *Chem. Rev.* 2019, 119, 1058-1137. (c) H. Ullah, V. Previtali, H. B. Mihigo, B. Twamley, M. K. Rauf, F. Javed, A. Waseem, R. J. Baker, I. Rozas, Structure-activity relationships of new Organotin(IV) anticancer agents and their cytotoxicity profile on HL-60, MCF-7 and HeLa human cancer cell lines. *Eur. J. Med. Chem.* 2019, 181, 111544.
- 5 (a) S. Keller, Y. Ching Ong, Y. Lin, K. Cariou, G. Gasser, A tutorial for the assessment of the stability of organometallic complexes in biological media. *J. Organomet. Chem.* 2020, 906, 121059. (b) C. Berg, S. Chari, K. Jurgaityte, A. Laurora, M. Naldony, F. Pope, D. Romano, T. Medupe, S. Prince, S. Ngubane, J. Baumgartner, B. Blom, Modulation of the solubility properties of arene ruthenium complexes bearing stannyl ligands as potential anti-cancer agents. *J. Organomet. Chem.* 2019, 891, 12-19. (c) G. Bresciani, N. Busto, V. Ceccherini, M. Bortoluzzi, G. Pampaloni, B. Garcia, F. Marchetti, Screening the biological properties of transition metal carbamates reveals gold(I) and silver(I) complexes as potent cytotoxic and antimicrobial agents, *J. Inorg. Biochem.* 2022, 227, 111667.
- 6 (a) U. Basu, M. Roy, A. R. Chakravarty, Recent advances in the chemistry of iron-based chemotherapeutic agents. *Coord. Chem. Rev.* 2020, 417, 213339. (b) W. A. Wani, U. Baig, S. Shreaz, R. A. Shiekh, P. F. Iqbal, E. Jameel, A. Ahmad, S. H. Mohd-Setapar, M. Mushtaque, I. Ting Hun, Recent advances in iron complexes as potential anticancer agents. *New J. Chem.* 2016, 40, 1063-1090. (c) A. Valente, T. S. Morais, R. G. Teixeira, C. P. Matos, A. I. Tomaz, M. H. Garcia, Ruthenium and iron metallodrugs: new inorganic and organometallic complexes as prospective anticancer agents. *Synth. Inorg. Chem.* 2021, Chapter 6, Elsevier Ed.
- 7 R. Crichton in "Iron Metabolism – From Molecular Mechanisms to Clinical Consequences", 2016, Wiley, 4th Ed.
- 8 (a) M. Patra, G. Gasser, The medicinal chemistry of ferrocene and its derivatives. *Nat. Chem. Rev.* 2017, 1, 66. (b) S. Sansook, S. Hassell-Hart, C. Ocasio, J. Spencer, Ferrocenes in medicinal chemistry; a personal perspective. *J. Organomet. Chem.* 2020, 905, 121017. (c) B. Sharma, V. Kumar, Has Ferrocene Really Delivered Its Role in Accentuating the Bioactivity of Organic Scaffolds? *J. Med. Chem.* 2021, 64, 16865 – 16921.

-
- 9 For ferrocene compounds tested in vivo, see: (a) S. Daum, V. F. Chekhun, I. N. Todor, N. Yu. Lukianova, Y. V. Shvets, L. Sellner, K. Putzker, J. Lewis, T. Zenz, I. A. M. de Graaf, G. M. M. Groothuis, A. Casini, O. Zozulia, F. Hampel, A. Mokhir, Improved Synthesis of N- Benzylaminoferrocene-Based Prodrugs and Evaluation of Their Toxicity and Antileukemic Activity. *J. Med. Chem.* 2015, 58, 2015–2024. (b) Q. Cheng, T. Zhou, Q. Xia, X. Lu, H. Xu, M. Hu, S. Jing, Design of ferrocenylseleno-dopamine derivatives to optimize the Fenton-like reaction efficiency and antitumor efficacy, *RSC Adv.*, 2021, 11, 25477. (c) M. M. Milutinović, P. P. Čanović, D. Stevanović, R. Masnikosa, M. Vraneš, A. Tot, M. M. Zarić, B. Simović Marković, M. Misirkić Marjanović, L. Vučićević, M. Savić, V. Jakovljević, V. Trajković, V. Volarević, T. Kanjevac, A. Rilak Simović, Newly Synthesized Heteronuclear Ruthenium(II)/Ferrocene Complexes Suppress the Growth of Mammary Carcinoma in 4T1-Treated BALB/c Mice by Promoting Activation of Antitumor Immunity. *Organometallics* 2018, 37, 4250–4266. (d) L. V. Snegur, A. N. Rodionov, L. A. Ostrovskaya, M. M. Ilyin, A. A. Simenel, Ferrocene-modified imidazoles: One-pot oxalyl chloride-assisted synthesis, HPLC enantiomeric resolution, and in vivo antitumor effects. *Appl Organomet Chem.* 2022, e6681. (e) A. N. Rodionov, L. V. Snegur, Y. V. Dobryakova, M. M. Ilyin Jr, V. A. Markevich, A. A. Simenel, Administration of ferrocene-modified amino acids induces changes in synaptic transmission in the CA1 area of the hippocampus. *Appl Organometal Chem.* 2020, 34, e5276. (f) A. N. Rodionov, L. V. Snegur, A. A. Simenel, Yu. V. Dobryakova, V. A. Markevich, Ferrocene-modified amino acids: synthesis and in vivo bioeffects on hippocampus. *Russ. Chem. Bull. Int. Ed.* 2017, 66, 136–142.
- 10 (a) R. Mazzoni, M. Salmi, V. Zanotti, C-C Bond Formation in Diiron Complexes. *Chem. Eur. J.* 2012, 18, 10174-10194. (b) L. Biancalana, F. Marchetti, Aminocarbyne ligands in organometallic chemistry. *Coord. Chem. Rev.* 2021, 449, 214203. (c) J. Chen, R. Wang, Remarkable reactions of cationic carbyne complexes of manganese, rhenium, and diiron with carbonylmetal anions. *Coord. Chem. Rev.* 2002, 231, 109-149. (d) Knorr, M.; Jourdain, I. Activation of alkynes by diphosphine- and m-phosphido-spanned heterobimetallic complexes. *Coord. Chem. Rev.* 2017, 350, 217-247.
- 11 (a) V. Ritleng, M. J. Chetcuti, Hydrocarbyl Ligand Transformations on Heterobimetallic Complexes. *Chem. Rev.* 2007, 107, 797–858. (b) G. Li, D. Zhu, X. Wang, Z. Su, M. R. Bryce, Dinuclear metal complexes: multifunctional properties and applications. *Chem. Soc. Rev.* 2020, 49, 765-838. (c) B. S. Natinsky, C. Liu. Two are better than one. *Nat. Chem.* 2019, 11, 199–203. (d) M. E. Garcia, D. Garcia-Vivo, A. Ramos, M. A. Ruiz, Phosphinidene-bridged binuclear complexes. *Coord. Chem. Rev.* 2017, 330, 1-36.
- 12 G. Agonigi, M. Bortoluzzi, F. Marchetti, G. Pampaloni, S. Zacchini, V. Zanotti. Additions to Diiron Carbonyl Complexes Containing a Bridging Aminocarbyne Ligand: A Synthetic, Crystallographic and DFT Study. *Eur. J. Inorg. Chem.* 2018, 960–971.

-
- 13 (a) V. G. Albano, L. Busetto, F. Marchetti, M. Monari, S. Zacchini, V. Zanotti, *Organometallics* 2003, 22, 1326-1331. (b) G. Ciancaleoni, S. Zacchini, V. Zanotti, F. Marchetti, DFT Mechanistic Insights into the Alkyne Insertion Reaction Affording Diiron μ -Vinyliminium Complexes and New Functionalization Pathways. *Organometallics* 2018, 37, 3718–3731.
- 14 V. G. Albano, L. Busetto, F. Marchetti, M. Monari, S. Zacchini, V. Zanotti, Stereochemistry of the insertion of disubstituted alkynes into the metal aminocarbene bond in diiron complexes. *J. Organomet. Chem.* 2004, 689, 528–538.
- 15 D. Rocco, L. K. Batchelor, G. Agonigi, S. Braccini, F. Chiellini, S. Schoch, T. Biver, T. Funaioli, S. Zacchini, L. Biancalana, M. Ruggeri, G. Pampaloni, P. J. Dyson, F. Marchetti. Anticancer Potential of Diiron Vinyliminium Complexes. *Chem. Eur. J.* 2019, 25, 14801-14816.
- 16 G. Agonigi, L. K. Batchelor, E. Ferretti, S. Schoch, M. Bortoluzzi, S. Braccini, F. Chiellini, L. Biancalana, S. Zacchini, G. Pampaloni, B. Sarkar, P. J. Dyson and F. Marchetti, Mono-, Di- and Tetra-iron Complexes with Selenium or Sulphur Functionalized Vinyliminium Ligands: Synthesis, Structural Characterization and Antiproliferative Activity. *Molecules*, 2020, 25, 1656.
- 17 S. Schoch, M. Hadji, S. A. P. Pereira, M. L. M. F. S. Saraiva, S. Braccini, F. Chiellini, T. Biver, S. Zacchini, G. Pampaloni, P. J. Dyson, F. Marchetti, A Strategy to Conjugate Bioactive Fragments to Cytotoxic Diiron Bis-Cyclopentadienyl Complexes. *Organometallics* 2021, 40, 2516 – 2528.
- 18 S. Schoch, D. Iacopini, M. Dalla Pozza, S. Di Pietro, I. Degano, G. Gasser, V. Di Bussolo, F. Marchetti, Tethering Carbohydrates to the Vinyliminium Ligand of Antiproliferative Organometallic Diiron Complexes. *Organometallics* 2022, 41, 514-526.
- 19 S. Braccini, G. Rizzi, L. Biancalana, A. Pratesi, S. Zacchini, G. Pampaloni, F. Chiellini, F. Marchetti, Anticancer Diiron Vinyliminium Complexes: A Structure–Activity Relationship Study. *Pharmaceutics* 2021, 13, 1158.
- 20 D. Rocco, N. Busto, C. Pérez-Arnaiz, L. Biancalana, S. Zacchini, G. Pampaloni, B. Garcia, F. Marchetti, Antiproliferative and bactericidal activity of diiron and monoiron cyclopentadienyl carbonyl complexes comprising a vinyl-aminoalkylidene unit. *Appl Organomet Chem.* 2020, 34, e5923.
- 21 S. Braccini, G. Provinciali, L. Biancalana, G. Pampaloni, F. Chiellini, F. Marchetti, The Cytotoxic Activity of Diiron Bis-Cyclopentadienyl Complexes with Bridging C_3 -Ligands. *Appl. Sci.* 2021, 11, 4351.
- 22 (a) H. Ghareeb, N. Metanis, The Thioredoxin System: A Promising Target for Cancer Drug Development, *Chem. Eur. J.* 2020, 26, 10175 – 10184. (b) M. Bian, R. Fan, S. Zhao, W. Liu, Targeting the Thioredoxin System as a Strategy for Cancer Therapy, *J. Med. Chem.* 2019, 62, 7309 – 7321.
- 23 A. De Palo, S. Zacchini, G. Pampaloni, F. Marchetti. Construction of a Functionalized Selenophene-Allylidene Ligand via Alkyne Double Action at a Diiron Complex. *Eur. J. Inorg. Chem.* 2020, 3268–3276.

-
- 24 G. Agonigi, G. Ciancaleoni, T. Funaioli, S. Zacchini, F. Pineider, C. Pinzino, G. Pampaloni, V. Zanotti, F. Marchetti. Controlled Dissociation of Iron and Cyclopentadienyl from a Diiron Complex with a Bridging C3 Ligand Triggered by One-Electron Reduction. *Inorg. Chem.* 2018, 57, 15172–15186.
- 25 T. Y. Luh, Trimethylamine N-Oxide-A Versatile Reagent For Organometallic Chemistry. *Coord. Chem. Rev.* 1984, 60, 255-276.
- 26 (a) M. A. Esteruelas, J. Herrero, A. M. Lopez, M. Olivan, Alkyne-Coupling Reactions Catalyzed by $\text{OsHCl}(\text{CO})(\text{P}^i\text{Pr}_3)_2$ in the Presence of Diethylamine, *Organometallics* 2001, 20, 3202-3205. (b) G. Bresciani, M. Bortoluzzi, C. Ghelarducci, F. Marchetti, G. Pampaloni, Synthesis of α -alkylidene cyclic carbonates via CO_2 fixation under ambient conditions promoted by an easily available silver carbamate, *New J. Chem.*, 2021, 45, 4340-4346.
- 27 G. Bresciani, L. Biancalana, G. Pampaloni, S. Zacchini, G. Ciancaleoni, F. Marchetti, A Comprehensive Analysis of the Metal–Nitrile Bonding in an Organo-Diiron System, *Molecules* 2021, 26, 7088.
- 28 (a) J. N. L. Dennett, S. A. R. Knox, K. M. Anderson, J. P. H. Charmant, A. G. Orpen, The synthesis of $[\text{FeRu}(\text{CO})_2(\mu\text{-CO})_2(\text{Cp})(\text{Cp}^*)]$ and convenient entries to its organometallic chemistry. *Dalton Trans.* 2005, 63-73. (b) C. P. Casey, S. R. Marder, B. R. Adams, Interconversion of μ -Alkylidyne and μ -Alkenyl Diiron Complexes. *J. Am. Chem. Soc.* 1985, 107, 7700-7705. (c) G. Bresciani, S. Zacchini, G. Pampaloni, M. Bortoluzzi, F. Marchetti, η^6 -Coordinated ruthenabenzenes from three-component assembly on a diruthenium μ -allenyl scaffold. *Dalton Trans.* 2022, 51, 8390–8400.
- 29 For the sake of comparison, the ^{29}Si NMR resonance of $[\text{Co}_2(\text{CO})_6(\mu\text{-}\eta^2\text{:}\eta^2\text{-HCCSiMe}_3)]$ in CDCl_3 was found at 2.1 ppm. P. Galow, A. Sebal, B. Wrackmeyer, Darstellung und NMR-spektroskopie organometallisch substituierter dikobalthexacarbonyl-alkin-komplexe. *J. Organomet. Chem.* 1983, 259, 253-268.
- 30 Cisplatin in cancer therapy: Molecular mechanisms of action. S. Dasari, P. B. Tchounwou. *Eur. J. Pharmacol.* 2014, 740, 364–378.
- 31 M. Kono, A. Ochida, T. Oda, T. Imada, Y. Banno, N. Taya, S. Masada, T. Kawamoto, K. Yonemori, Y. Nara, Y. Fukase, T. Yukawa, H. Tokuhara, R. Skene, B.-C. Sang, I. D. Hoffman, G. P. Snell, K. Uga, A. Shibata, K. Igaki, Y. Nakamura, H. Nakagawa, N. Tsuchimori, M. Yamasaki, J. Shirai, S. Yamamoto, Discovery of $[\text{cis-3-}(\{(5R)\text{-5-}[(7\text{-Fluoro-1,1-dimethyl-2,3-dihydro-1H-inden-5-yl})\text{carbamoyl}]\text{-2-methoxy-7,8-dihydro-1,6-naphthyridin-6(5H-yl)}\})\text{carbonyl}]\text{cyclobutyl]acetic Acid (TAK-828F)}$ as a Potent, Selective, and Orally Available Novel Retinoic Acid Receptor-Related Orphan Receptor γT Inverse Agonist. *J. Med. Chem.* 2018, 61, 2973-2988.
- 32 G. Agonigi, L. Biancalana, M. G. Lupo, M. Montopoli, N. Ferri, S. Zacchini, F. Binacchi, T. Biver, B. Campanella, G. Pampaloni, V. Zanotti, F. Marchetti, Exploring the Anticancer Potential of Diiron Bis-

cyclopentadienyl Complexes with Bridging Hydrocarbyl Ligands: Behavior in Aqueous Media and In Vitro Cytotoxicity. *Organometallics* 2020, 39, 645-657.

- 33 (a) A. Pratesi, C. Gabbiani, E. Michelucci, M. Ginanneschi, A. M. Papini, R. Rubbiani, I. Ott, L. Messori. Insights on the mechanism of thioredoxin reductase inhibition by Gold N-heterocyclic carbene compounds using the synthetic linear Selenocysteine containing C-terminal peptide hTrxR(488-499): An ESI-MS investigation. *J. Inorg. Biochem.*, 2014, 136, 161–169. (b) L. Massai, A. Pratesi, J. Bogojeski, M. Banchini, S. Pillozzi, L. Messori, Ž. D. Bugarčić, Antiproliferative properties and biomolecular interactions of three Pd(II) and Pt(II) complexes. *J. Inorg. Biochem.*, 2016, 165, 1–6. (c) L. Chiaverini, A. Pratesi, D. Cirri, A. Nardinocchi, I. Tolbatov, A. Marrone, M. Di Luca, T. Marzo, D. La Mendola. Anti-staphylococcal activity of the auranofin analogue bearing acetylcysteine in place of the thiosugar: an experimental and theoretical investigation. *Molecules*, 2022, 27, 2578.
- 34 L. Biancalana, M. De Franco, G. Ciancaleoni, S. Zacchini, G. Pampaloni, V. Gandin, F. Marchetti, Easily Available, Amphiphilic Diiron Cyclopentadienyl Complexes Exhibit in Vitro Anticancer Activity in 2D and 3D Human Cancer Cells through Redox Modulation Triggered by CO Release. *Chem. Eur. J.* 2021, 27, 10169–10185.
- 35 (a) J. J. Gair, B. E. Haines, A. S. Filatov, D. G. Musaev, J. C. Lewis, Mono-N-protected amino acid ligands stabilize dimeric palladium(ii) complexes of importance to C–H functionalization, *Chem. Sci.* 2017, 8, 5746-5756. (b) M. Bortoluzzi, G. Bresciani, F. Marchetti, G. Pampaloni, S. Zacchini, MoCl₅ as an effective chlorinating agent towards α -amino acids: synthesis of α -ammonium-acylchloride salts and α -amino-acylchloride complexes, *Dalton Trans.* 2015, 44, 10030–10037.
- 36 P. Štarha, J. Vanco, Z. Trávníček, Platinum iodido complexes: A comprehensive overview of anticancer activity and mechanisms of action, *Coord. Chem. Rev.* 2019, 380, 103–135
- 37 Note that the cancer cell selectivity parameter **Sel** is normalized with respect to cisplatin (IC₅₀ values measured for the same cell lines in the same batch of measurements). This data treatment is necessary because of the different cell lines used (HEK and Balb). Separate analyses of A2870/HEK and A2870/Balb selectivity would significantly reduce the number of compounds in each group, hence the associated R¹-R⁴ variability.
- 38 T. Österberg, U. Norinder. Prediction of polar surface area and drug transport processes using simple parameters and PLS statistics. *J. Chem. Inf. Comput. Sci* 2000, 40.6, 1408-1411.
- 39 See for instance: (a) S. Segan, N. Terzic-Jovanovic, D. Milojkovic-Opsenica, J. Trifkovic, B. Solaja, D. Opsenica, Correlation study of retention data and antimalarial activity of 1,2,4,5-mixed tetraoxanes with their molecular structure descriptors and LSER parameters, *J. Pharm. Biomed. Anal.* 2014, 97, 178–183. (b) L. G. Ramírez-Palma, C. R. García-Jacas, J. C. García-Ramos, R. Almada-Monter, R. Galindo-Murillo, F. Cortes-Guzman, Pharmacophoric sites of anticancer metal complexes located using quantum topological

-
- atomic descriptors, *J. Mol. Struct.* 2020, 1204, 127480. (c) J.-Z. Qian, B.-C. Wang, Yi Fan, J. Tan, H. J. Huang, QSAR study of flavonoid–metal complexes scavenging $O_2^{\cdot-}$. *J. Coord. Chem.* 67, 2014, 2867–2884
- 40 R. Mazzoni, A. Gabiccini, C. Cesari, V. Zanotti, I. Gualandi, D. Tonelli, Diiron Complexes Bearing Bridging Hydrocarbyl Ligands as Electrocatalysts for Proton Reduction, *Organometallics* 2015, 34, 3228–3235.
- 41 The three models include different number of observations (x_i, y_i), depending on the available data (Table S1); more specifically, 42 compounds for Log P_{ow} , 48 for **Tox** (A2780) and 46 for **Sel**.
- 42 M. L. Landry, J. J. Crawford, Log D Contributions of Substituents Commonly Used in Medicinal Chemistry, *ACS Med. Chem. Lett.* 2020, 11, 72–76
- 43 F. Menges, "Spectragryph - optical spectroscopy software", Version 1.2.5, @ 2016-2017, <http://www.effemm2.de/spectragryph>.
- 44 G. R. Fulmer, A. J. M. Miller, N. H. Sherden, H. E. Gottlieb, A. Nudelman, B. M. Stoltz, J. E. Bercaw, K. I. Goldberg, NMR Chemical Shifts of Trace Impurities: Common Laboratory Solvents, Organics, and Gases in Deuterated Solvents Relevant to the Organometallic Chemist, *Organometallics* 2010, 29, 2176–2179.
- 45 W. Willker, D. Leibfritz, R. Kerssebaum, and W. Bermel, *Magn. Reson. Chem.* 1993, 31, 287-292.
- 46 V. G. Albano, L. Busetto, M. Monari, V. Zanotti. Reactions of acetonitrile di-iron π -aminocarbyne complexes; synthesis and structure of $[Fe_2(\mu-CNMe_2)(\mu-H)(CO)_2(Cp)_2]$. *J. Organomet. Chem.* 2000, 606, 163–168.
- 47 T. Rundlöf, M. Mathiasson, S. Bekiroglu, B. Hakkarainen, T. Bowden, T. Arvidsson, Survey and qualification of internal standards for quantification by 1H NMR Spectroscopy. *J. Pharm. Biomed. Anal.* 2010, 52, 645–651.
- 48 N. M. Rice, H. M. N. H. Irving, M. A. Leonard, Nomenclature for liquid-liquid distribution (solvent extraction). *Pure Appl. Chem.* 1993, 65, 2373-2396.
- 49 a) OECD Guidelines for Testing of Chemicals. In OECD, Paris: 1995; Vol. 107. b) J. C. Dearden,; G. M. Bresnen, The Measurement of Partition Coefficients, *Quant. Struct.-Act. Relat.* 1988, 7, 133-144.

